European Journal of Medicinal Chemistry 271 (2024) 116365

Contents lists available at ScienceDirect

European Journal of Medicinal Chemistry

journal homepage: www.elsevier.com/locate/ejmech

Research paper

Identification of a new bisindolinone arresting IGROV1 cells proliferation

Rita Morigi [a,1], Chiara Zalambani [b,1], Giovanna Farruggia [b,c], Laura Verardi [b], Daniele Esposito [a], Alberto Leoni [a], Francesca Borsetti [b], Manuela Voltattorni [b], Laura Zambonin [b], Luca Pincigher [b], Natalia Calonghi [b], Alessandra Locatelli [a,*]

[a] Department of Pharmacy and Biotechnology, Alma Mater Studiorum—University of Bologna, Via Belmeloro 6, 40126, Bologna, Italy
[b] Department of Pharmacy and Biotechnology, Alma Mater Studiorum—University of Bologna, Via Irnerio 48, 40126, Bologna, Italy
[c] INBB-Biostructures and Biosystems National Institute, 00136, Rome, Italy

ARTICLE INFO

Keywords:
Indolinone scaffold
Knoevenagel reaction
Ovarian cancer
QPI
Cyclin D1
siRNA

ABSTRACT

In an initial screening, a series of novel Knoevenagel adducts were submitted to the National Cancer Institute for evaluation of antitumor activity in human cell lines. In particular, compound **5f** showed remarkable selectivity against IGROV1, an ovarian cancer cell line, without affecting healthy human fibroblast cells. Analyses of cytotoxicity, cell proliferation, cell migration, epigenetic changes, gene expression, and DNA damage were performed to obtain detailed information about its antitumor properties. Our results show that **5f** causes proliferation arrest, decrease in motility, histone hyperacetylation, downregulation of cyclin D1 and α5 subunit of integrin β1 gene transcription. In addition, **5f** treatment reduces transcript and protein levels of cyclin D1, which increases sensitivity to ionizing radiation and results in DNA damage comparable to cyclin D1 gene silencing.

1. Introduction

Cancer is a complex disease in which a variety of genomic and physiological changes constantly occur in tumor tissue, complicating the treatment and management of the disease [1]. Most cancer patients initially respond very well to chemotherapy, but a significant proportion of these patients relapse due to the development of treatment resistance [2,3].

Ovarian cancer is the second most common and deadliest gynecologic malignancy in the Western world. The reason for this is the lack of safe methods for early detection of this disease. This fact explains why about 70% of cases are diagnosed at an advanced stage and consequently are associated with a poor prognosis. Advanced stage ovarian cancer is incurable in most cases, but thanks to advances in surgical techniques and the development of new drugs, it's recently becoming more of a chronic disease [4].

Only 15% of ovarian cancers is recognized at an early or localized stage, lowering the chance of survival. The majority of this kind of tumors has an epithelial origin and treatment primarily consists of surgery and cytoreduction, followed by chemotherapy with platinum and taxanes [5]. Unfortunately, although most tumors initially respond to this treatment, advanced stage patients relapse within approximately 16 months. In addition to conventional chemotherapy, new therapeutic approaches that take advantage of breakthrough in our understanding of the pathophysiology of ovarian cancer are needed to improve these outcomes.

The 2-indolinone scaffold represents a widely used pharmacophore in the design process of new anticancer agents, also due to its promising pharmacological activity [6]. Our research group has been engaged in the synthesis of 2-indolinone derivatives as antiproliferative agents for several years [7–10]. In particular, some studies have been focused on Knoevenagel adducts bearing two indole nuclei linked to an aromatic core [11–13] and have allowed the identification of derivatives endowed with interesting antiproliferative activity profiles. The promising results previously obtained prompted us to pursue a deeper exploration of the chemical space for these bis-indole derivatives by planning the synthesis of a new series of 37 analogues. Specifically, new substituents were introduced on the indole nuclei linked to a benzene ring (compounds **5** and **7**, Scheme 1) such as fluorine at position 4 or 5 (compounds **5a**, **5d**, **7a**, **7d**) or benzyl at the indolinone nitrogen (compounds **5g**, **5i**, **7g**, **7i**). For these compounds, the effect of the chlorine position shift (compounds **5c**, **5f**, **7f**) and of the introduction of more than one chlorine or methoxy group (compounds **5b**, **5c**, **7j**) was also studied to compare the activity with previously studied derivatives

* Corresponding author.
E-mail address: alessandra.locatelli@unibo.it (A. Locatelli).
[1] These authors contributed equally to this work.

https://doi.org/10.1016/j.ejmech.2024.116365
Received 8 January 2024; Received in revised form 14 March 2024; Accepted 27 March 2024
Available online 2 April 2024

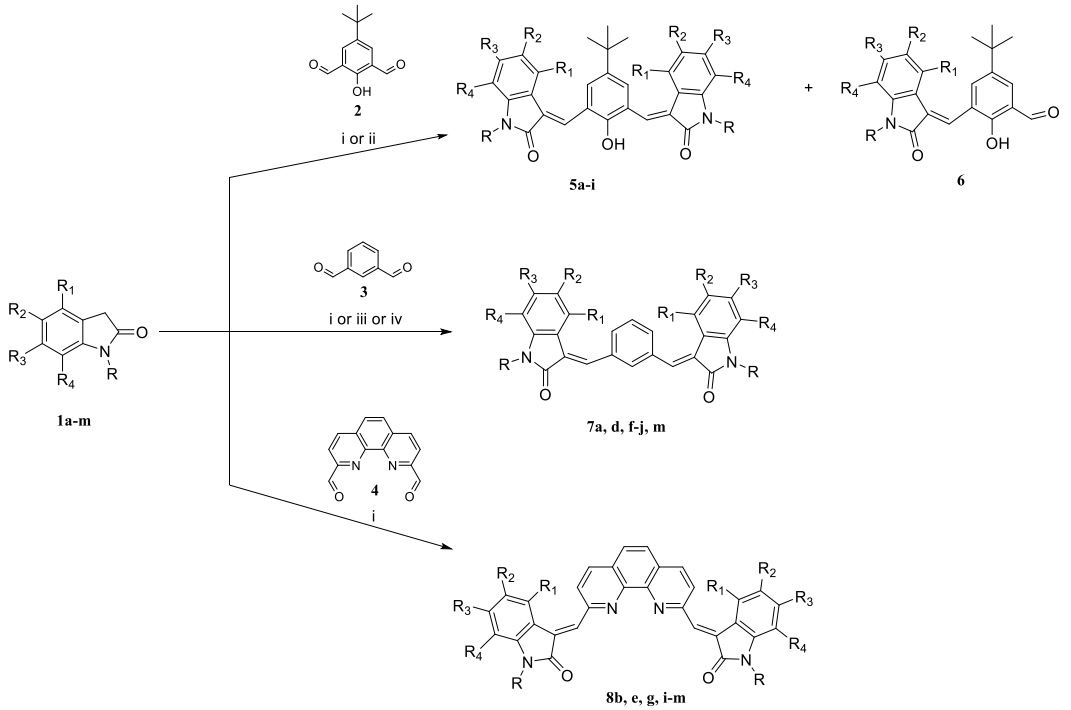

Compound	Starting compound	R	R_1	R_2	R_3	R_4
5a	**1a**	H	F	H	H	H
5b	**1b**	H	OCH_3	OCH_3	OCH_3	H
5c	**1c**	H	Cl	H	H	Cl
5d	**1d**	H	H	F	H	H
5e	**1e**	CH_3	H	OCH_3	H	H
5f	**1f**	H	H	H	Cl	H
5g	**1g**		H	H	H	H
5h	**1h**	H	H	OH	CH_3	H
5i	**1i**	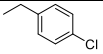	H	H	H	H
6	**1h**	H	H	OH	CH_3	H
7a	**1a**	H	F	H	H	H
7d	**1d**	H	H	F	H	H
7f	**1f**	H	H	H	Cl	H
7g	**1g**		H	H	H	H
7h	**1h**	H	H	OH	CH_3	H
7i	**1i**	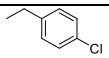	H	H	H	H
7j	**1j**	H	OCH_3	H	H	OCH_3
7m	**1m**	H	H	OCH_3	CH_3	H
8b	**1b**	H	OCH_3	OCH_3	OCH_3	H
8e	**1e**	CH_3	H	OCH_3	H	H
8g	**1g**		H	H	H	H
8i	**1i**	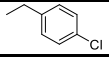	H	H	H	H
8j	**1j**	H	OCH_3	H	H	OCH_3
8k	**1k**	H	H	Cl	H	H
8l	**1l**	CH_3	H	Cl	H	H
8m	**1m**	H	H	OCH_3	CH_3	H

Scheme 1. Synthetic route for obtaining the new derivatives **5a–i**, **6**, **7a**, **d**, **f-j**, **m**, **8b**, **e**, **g**, **i–m.** Reagents and conditions: (**i**) CH_3OH, piperidine; (**ii**) CH_3CH_2OH, HCl; (**iii**) CH_3COOH, HCl; (**iv**) toluene,4-toluenesulfonic acid.

(see compounds **16j, 16k**, **18j**, **18k** in [12] and compounds **4b**, **4c**, **5b**, **5c** in [13]). Moreover, a methyl group was added at the 6 position when the 5 position bears a hydroxy (compounds **5h**, **7h**) or a methoxy group (compound **7m**). In an attempt to obtain compound **5h**, the mono-indolinone derivative **6** was isolated from the reaction mixture, characterized and tested to get preliminary information about the lack of one indolinone nucleus. Regarding phenanthroline derivatives **8** (Scheme 1), the simultaneous presence of more than one methoxy group on the indolinone nuclei (compounds **8b**, **8j**) was studied, together with the effect of a methyl group at position 6 (compound **8m**). In addition, the shift of the chlorine from position 4 (compound **19k** in [12]) to position 5 (compound **8k**) and the effect of a substituent, either small as a methyl (compounds **8e**, **8l**) or bulky as a benzyl (compounds **8g**, **8i**) at the indolinone nitrogen were also investigated. Finally, for compounds bearing the pyrroloindoledione core (compounds **11**, Scheme 2), position 5 of the indoles was substituted with a methoxy or a dimethylamino group, which in previous studies had given good results with the pyridine core [11]. Furthermore, the addition of a methyl at position 6 (compounds **11r**, **11u**, **11v**) or the lack of the chlorine at position 2 of the indole (compound **11p**) was also studied together with the introduction at the indole nitrogen of a methyl, a phenyl, a benzyl or a p-chloro-benzyl group (compounds **11q**, **11r**, **11s**, **11t**, **11w**, **11x**).

Protocols studied in collaboration with the National Cancer Institute (NCI, Bethesda, MD) made possible the evaluation of the antitumor activity of the synthetized compounds. Afterwards, we focused our study on the effect of compound **5f** on the ovarian cancer cell line IGROV1. We used the technique of Quantum Phase Imaging (QPI) to investigate the effects on cell proliferation, cell morphology and motility. Furthermore, we studied the modulation of histone acetylation and genes expression. In addition, we focused on the expression of cyclin D1, which is known to protect against DNA damage.

2. Results and discussion

2.1. Chemistry

The new derivatives **5a–i**, **6**, **7a**, **d**, **f-j**, **m**, **8b**, **e**, **g**, **i–m**, **11n-x** (Schemes 1 and 2) were obtained through Knoevenagel condensation, involving a carbonyl and a methylene group where the latter is activated by a neighboring electron withdrawing substituent. The classes of compounds reported in Schemes 1 and 2 represent our continued synthetic efforts using the Knoevenagel reaction. In the first case (Scheme 1, compounds **5–8**), the formyl groups take part to the formation of the main scaffold, with the two activated methylene groups that will contribute to the formation of the two-sided indole wings. In the second case (Scheme 2, compounds **11**), the substitution was opposite, showing the contribution of the methylene groups to the main core (pyrrolo [3,2-f]indole-2,6(1H,3H)-dione ring) and the carbonyl groups on the sides of the product structures. The new analogues were obtained performing analogue procedures to the ones described for the previously published

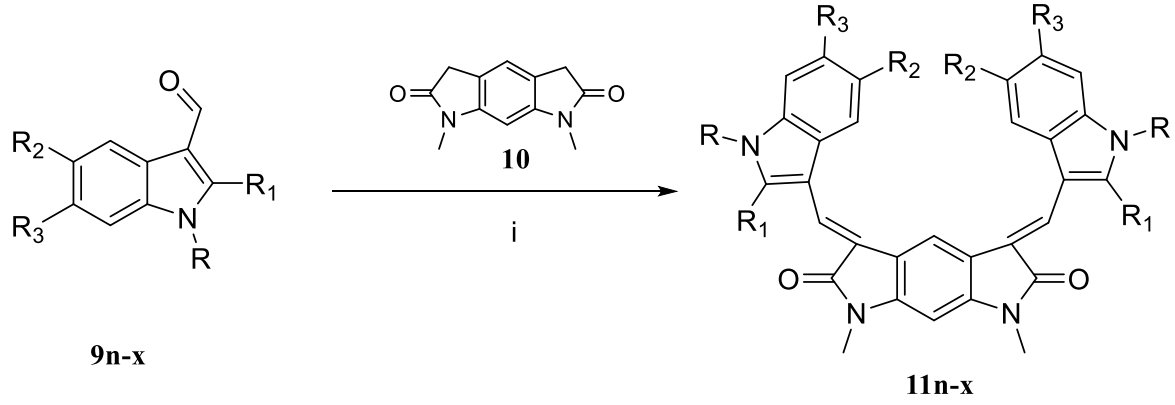

Compound	R	R_1	R_2	R_3
11n	H	Cl	$N(CH_3)_2$	H
11o	H	Cl	OCH_3	H
11p	H	H	OCH_3	H
11q	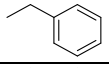	Cl	H	H
11r	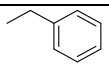	Cl	OCH_3	CH_3
11s	CH_3	Cl	H	H
11t		Cl	H	H
11u	H	Cl	OH	CH_3
11v	H	Cl	OCH_3	CH_3
11w	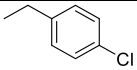	Cl	OCH_3	H
11x	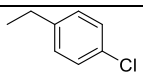	Cl	OCH_3	CH_3

Scheme 2. Synthetic route for obtaining new derivatives **11n-x.**Reagents and conditions: (**i**) CH_3OH, piperidine.

compounds [11–13]: indolinones **1** or **10** were treated with appropriate carbaldehyde **2**–**4** or **9** with piperidine (method 1). Since these conditions were not always successful, for the synthesis of compound **5c**, ethanol and HCl conc. have been used (method 2); for compounds **7a**, **d**, **f**, **j**, a mixture of acetic acid/hydrochloride was used (method 3); for compound **7g**, the reaction was performed with toluene and p-toluensulfonic (method 4).

IR, ^{1}H NMR and ESI-MS analysis confirmed the structures of the final compounds, which were identified as mostly pure geometrical isomers, although they did not show same stability in DMSO-d_6 solvent. In fact, almost all the analogues in solution undergo isomerization leading to complex mixtures of the three isomers (EE, EZ, ZZ). The long times of acquisition required to obtain complete ^{13}C NMR spectra, because of the high number of quaternary carbons, led to crowded ^{13}C NMR spectra ultimately meaningless. For this reason, the ^{13}C NMR spectrum was described only for the studied compound **5f** which, during the ^{13}C NMR spectrum acquisition, underwent only slight isomerization.

The analysis of the ^{1}H NMR spectra showed that for most of the compounds the geometrical configuration of the two centers is the same, since the couple of NH groups and the other couples of indole protons give a single signal. Only in compounds **5b** and **5c** the two centers have different configurations as the signals of the proton of the two indole nuclei and of the two methine bridges are different (Chart 1).

The geometrical configuration of compounds **11** was studied by performing NOE (Nuclear Overhauser Effect) experiments on compound **11o** to determine whether the methine bridge and the proton of the aromatic core are close in space (Z configuration) or not (E configuration). The irradiation of –CH = protons of the methine bridges at 7.46 ppm did not produce any effect on other protons and the irradiation of ind-4 (5.83 ppm) produced NOE only at the aromatic core protons (singlet 6.55 ppm). These data are in agreement with the *E* configuration (Chart 2).

As far as compounds **5–8** are concerned, since the peaks of the ^{1}H NMR spectra were too near for significant NOE experiments, we compared the common features of analogue derivatives [13]. On this basis, we believe that these compounds also have the *E* configuration.

2.2. Biological studies

2.2.1. Effects in cultured human tumor cell lines

In order to evaluate the potential antitumor activity of the new compounds, they were involved in the Developmental Therapeutics Program (DTP) at the National Cancer Institute (NCI) (http://dtp.nci.nih.gov). In the first place, the compounds were preliminarily tested at a single high concentration (10 μM) in an NCI 60 cell panel approach (NCI 60 Cell One-Concentration Screen). The tests were performed using different cancer cell lines including melanoma, leukemia, colon, lung, ovary, kidney, breast, prostate, and central nervous system cancers. During this first round of experiments, a set of criteria given by historical DTP screening data was chosen to successfully recognize compounds with an actual antiproliferative activity and only the compounds responding to these threshold inhibition criteria in a minimum number of cancer cell lines were considered to progress to the full 5-concentration assay. Values of percentage of growth of treated cells relative to the control after 48 h incubation were used to express the results and the one-concentration data corresponds to a mean outcome of the percent growth of treated cells (unpublished results). The full 5-concentration assay was then performed with seventeen of the new compounds. DMSO was used as solvent and five concentrations at ten-fold dilutions were used, with the highest one of 100 μM. Results are reported in Table 1 (vincristine is reported for comparison purposes) with three main endpoints: the 50% growth inhibitory power (GI_{50}), the cytostatic effect (TGI = Total Growth Inhibition) and the cytotoxic effect (LC_{50}). In some cases, the test was repeated and the data in Table 1 is the result a mean of the two experiments.

2.2.2. Structure–Activity Relationships

By comparing the results obtained in the tests performed at the NCI, it was possible to obtain some Structure–Activity Relationships (SAR) information. As far as the studied core is concerned, in general all the nuclei proved to be effective when the oxindoles or the chloroindoles were properly substituted.

The introduction of a bulky substituent, such as a phenyl, a benzyl, a p-chlorophenyl on the nitrogen of the indolinone nucleus (compounds **5g**, **7g**, **8g**, **5i**, **7i**, **8i**) or at the nitrogen of the chloroindole (compounds **11q**, **11r**, **11t**, **11w**, **11x**) was detrimental for the antiproliferative activity: indeed, none of these compounds passed the preliminary assay and was evaluated in the full 60 cell lines panel.

In compounds bearing a benzene core (compounds **5** and **7**) the introduction of a halide (fluorine or chlorine) on the oxindoles led to active compounds showing mean GI_{50} values in the low micromolar range (compounds **5a**, **7a**, **5d**, **7d**, **5f**, **7f**), thus confirming the good effect of one halide at either position 4, 5 or 6 of the 2-indolinones. In fact, similar results had been obtained with previously studied 4-chloro derivatives (see compounds **16k**, and **18k** in Ref. [12]) and 5-bromo or 5-chloro derivatives (see compounds **4b**, **4c**, **5b**, **5c** in Ref. [13]). On the other hand, the substitution with of two chlorines at positions 4 and 7 of the oxindoles led to an inactive compound (**5c**). Among halogenated derivatives **5**, compound **5f** showed an interesting activity profile and was further studied to better understand its mechanism of action.

Derivatives bearing the benzene core condensed with two 5-hydroxy-6-methyl-2-indolinones (compounds **5h** and **7h**) did not pass the preliminary test. On the contrary, the corresponding mono-condensed analogue **6**, tested on the full 60 cell line panel, showed a good antiproliferative activity (mean GI_{50} value 1.91 μM), which may be attributed to the presence of the formyl group. Interestingly, the introduction of three methoxy groups on the oxindoles gave good results in the analogue bearing a tert-butyl-hydroxy-phenyl core (**5b**), which showed a mean GI_{50} value of 1.95 μM and therefore proved to be more potent than the corresponding 5-methoxy analogue (compound **18j** in Ref. [12], mean GI_{50} = 5.7 μM).

Regarding phenanthroline derivatives (compounds **8**), the shift of the chlorine from position 4 to position 5 led to a slight increase of the antiproliferative activity. Indeed, for the previously reported 4-chloro analogue (compound **19k** in Ref. [12]) the mean GI_{50} value was 8.10 μM, whereas compound **8k** showed mean GI_{50} of 2.63 μM, similar to that

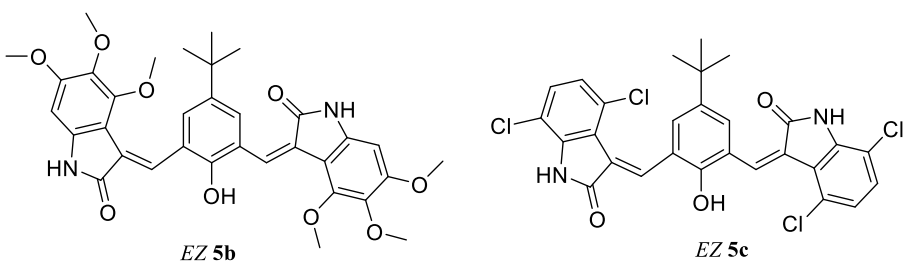

Chart 1. Chemical structures of compounds **5b**, **5c**.

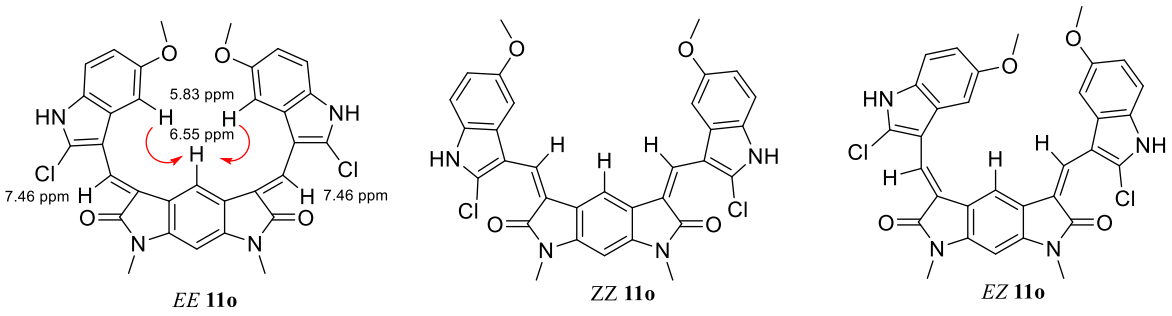

Chart 2. NOE correlations proved **11o** is the *EE* isomer.

of previously described analogues bearing the benzene core (see compounds **4c** and **5c** [13]). On the other hand, the simultaneous introduction of a methyl at the oxindole nitrogens (compound **8l**) brought a loss of activity, whereas this modification was tolerated with the benzene core (see compounds **4d** and **5d** [13]). For phenanthroline derivatives, the simultaneous introduction of a methoxy group at position 4, 5 and 6 of the oxindoles led to a slight drop in activity: compound **8b** showed a mean GI_{50} value of 12.88 μM, while for the 5-methoxy analogue (compound **19j** in Ref. [12]) the mean GI_{50} value was 3.5 μM. Better results were obtained with the addition of a methyl group at nitrogen or at position 6 of the oxindoles, indeed, compounds **8e** and **8m** showed mean GI_{50} values of 2.63 μM and 5.13 μM, respectively.

Even in derivatives bearing the pyrroloindole-dione core, the presence of a methoxy group at position 5 of the two indoles led to interesting compounds, but only if a chlorine was also present in position 2. Indeed, compounds **11o** and **11v** showed mean GI_{50} value of 2.04 μM, whereas compound **11p** did not pass the NCI preliminary test.

2.2.3. *Effect on cell viability*

More common neoplastic pathologies such as breast cancer, cervical cancer, and colorectal cancer have a good prognosis because they can be diagnosed early and treated according to the best protocols. However, this is not the case for ovarian cancer, which remains the deadliest gynecologic malignancy in women despite all treatment advances. Grunewald and Ledermann stressed the importance of changing the treatment protocol for ovarian cancer. While surgery and chemotherapy remain essential, new targeted therapies, both in combination with chemotherapy and alone, have led to significant improvements in survival, suggesting that a "one-size-fits-all" protocol for ovarian cancer is no longer acceptable [14]. Targeted therapy is the most rapidly evolving type of cancer treatment. It involves the use of drugs or small molecules designed to block tumor growth.

As shown in Table 1, all compounds of series **5**, with the exception of compound **5d**, show good antitumor activity in ovarian cancer acting at very low concentrations with a GI_{50} between 1.95 and 2.69 μM.

For this reason, we decided to continue this study using the IGROV1 cell line as a cell model and the molecule **5f**.

IGROV1 is a line originating from an ovarian carcinoma of a 47-year-old woman, is at grade 2 and stage III with highly tumorigenic properties. A paracentric inversion of chromosome 3 and a translocation between chromosomes 2 and 5 are cytogenetic markers characterizing IGROV1, while the patient's karyotype is normal [15]. TP53, BRCA1 and BRCA2 genes are mutated, but BRCA2 mutation is silent; in total there are three mutated genes in homologous recombination repair pathway [15,16]. These characteristics make IGROV1 cell line a suitable experimental model for treatment of human ovarian carcinomas and for biological studies on human solid tumors.

In addition, the effects induced by **5f** have also been studied in a normal cell line, HDFa.

IGROV1 and a non-transformed line, HDFa, were exposed to **5f** for 24 h, then potential cytotoxic activity was assessed by MTT assay. Cytotoxic activity was expressed as IC_{50} value, which is the concentration of the compound that reduces cell viability by 50%. The results reported in Fig. 1A and B and Table 2 indicate that **5f** showed some degree of cytotoxicity in IGROV1, with IC_{50} values of 6.06 μM ± 0.01, while in HDFa it showed biological activity with higher IC_{50} values of 21.93 μM ± 0.13.

The selectivity index (SI) of 3.64 was reported in Table 2, indicating that **5f** has higher efficacy against cancer cells than toxicity against normal cells.

2.2.4. *Effects on cell proliferation and motility*

Assessing the average cellular response to drug treatment by parameters such as reduction in cell viability, death by apoptosis, or effects on the ability to form colonies does not provide completely exhaustive information, especially in cancer. The rare cells that show resistance to the therapeutic are likely those that fall outside the average and are therefore masked by their response. By treating each cell as a data point, it is possible to identify the characteristics of resistant cells by obtaining more information that can help in understanding therapy resistance and tumor recurrence.

Phasefocus Livecyte is an inverted system for live cell imaging. This microscope is equipped with QPI, a label-free technique that uses phase shift information to produce high-contrast, detailed images of cells with low phototoxicity and photobleaching. Recent advances in QPI techniques have made it possible to observe subtle time-dependent changes on photomicrographs, such as in cell mass distribution, cell density, cell membrane microfractures, nuclear shape, homogeneity of cell content, and many other parameters that can be observed without fixation, labeling, or cell harvesting [17].

Fig. 2 shows the images of IGROV1 and HDFa at 0, 24, and 48 h after treatment. As it can be observed, **5f** in IGROV1 strongly inhibits proliferation, although the cells are still attached after 48 h of treatment, indicating that they are still viable.

Effects on cell proliferation were analyzed by cell number and doubling time (DT) measurements.

Treatment with compound **5f** at a concentration of 5 μM leads to a strong anti-proliferative effect on IGROV1, as shown both by cell count (Fig. 3A) and cell confluence (Fig. 3B) graphs and especially by the DT histogram (Fig. 3C). DT in IGROV1 is not evaluable, being a negative value. However, even if there is a decrease in cell numbers in the first 24 h of treatments, then there is a very slight restart of the cell growth, but characterized, in this period of time, by DT extremely high, increasing from 23.9 ± 2.4 h of the controls to 113.3 ± 37.7, indicating that cells are not dying but are severely inhibited in their growth, (data not shown).

In contrast, the antiproliferative effect is not as strong in normal fibroblasts. After 48 h, treatment with **5f** increases DT from 35 to 56 h, respectively, indicating that these cells slowly proliferate but they do not arrest (Fig. 3C).

Motility assays are indispensable tools for measuring the movement of cells. In a random single cell motility assay, cells move independently due to their dispersed state. Because Livecyte tracks cells individually, the motility of each cell can be measured automatically throughout the assay. Fig. 4 shows motility analysis with measurements of mean velocity and metrics describing direction and immediacy of motion, such as displacement and directionality. It is evident that **5f** decreases individual cell displacement and velocity at a higher rate in IGROV1 (Fig. 4A and C) compared to HDFa cells (Fig. 4 B and D). Directionality seems less affected by treatment. It is interesting to note that even if some IGROV1 cells remain alive after 24 h of treatment with **5f**, however their motility is strongly inhibited for the entire time considered.

These data suggest that the prolonged doubling times observed in HDFa cells after 24 h treatment with **5f** may be due to a decreased proliferation rate or increased cell death without temporal consequences. In contrast, treatment with **5f** of IGROV1 cells leads to more impressive biological effects by permanently altering important cellular parameters such as cell number, and DT. For this reason, studies with **5f** in IGROV1 cells were continued.

Subsequent studies were designed to clarify whether **5f**-induced antiproliferative activity is responsible for the delay of a specific phase of the cell cycle.

To this end, IGROV1 cells were treated with 5 μM **5f** for 24 h, then stained with PI and subjected to flow cytometric analysis. Fig. 5 shows that IGROV1 cells treated with **5f** exhibit a significant increase in G0/G1 phase by approximately 13.4% ± 0.8, followed by a decrease in S and G2/M phases by approximately 21.2% ± 0.9 and 11.9% ± 0.6, respectively.

2.2.5. *Epigenetic modifications*

Epigenetic changes are used to diagnose individual patients more accurately and specifically. In the context of precision medicine, several

Table 1
The results for the new compounds were expressed as growth inhibition, cytostatic and cytotoxic activity (μM) in nine subpanels at five concentrations.

Comp [b]	Modes	Leukemia	NSCLC	Colon	CNS	Melanoma	Ovarian	Renal	Prostate	Breast	MG-MID[c]
5a	GI_{50}	1,58	2,14	2,19	2,09	2,29	1,95	2,45	2,75	2,04	2,14
	TGI	4,79	5,89	6,46	6,46	5,5	5,89	7,24	9,77	8,51	6,46
	LC_{50}	22,91	15,85	16,98	20,42	13,18	15,49	20,42	36,31	33,88	19,5
5b	GI_{50}	2,19	1,95	1,91	1,62	1,82	2,19	2,19	1,91	1,86	1,95
	TGI	6,03	4,27	3,89	3,31	3,63	5,13	4,9	4,47	4,9	4,37
	LC_{50}	60,26	14,79	8,13	6,76	8,13	25,12	14,79	12,59	50,12	15,49
5d	GI_{50}	3,09	4,17	4,68	2,95	3,02	4,07	4,68	3,89	3,8	3,8
	TGI	12,02	16,22	14,79	12,02	9,77	15,85	14,13	15,14	19,5	13,8
	LC_{50}	60,26	47,86	42,66	39,81	33,88	47,86	38,9	4,74	46,77	42,66
5e	GI_{50}	2,82	2,34	2,19	1,91	1,86	2,45	2,51	3,09	2,24	2,24
	TGI	20,42	6,61	4,79	4,9	3,98	7,24	8,32	12,88	6,17	6,61
	LC_{50}	100	31,62	16,98	16,6	9,55	28,18	30,2	67,61	36,31	25,7
5f	GI_{50}	2,45	3,63	4,17	2,75	2,82	2,69	2,69	3,63	2,95	3,02
	TGI	18,62	14,45	13,18	11,75	8,51	10	11,22	13,49	13,18	12,02
	LC_{50}	97,72	47,86	37,15	41,69	30,9	30,9	35,48	38,02	48,98	41,69
6	GI_{50}	0,68	3,47	3,31	1,2	1,78	1,95	2,57	0,87	1,82	1,91
	TGI	3,72	12,88	11,48	10	5,75	9,55	11,48	4,57	14,79	8,91
	LC_{50}	81,28	51,29	38,02	72,44	37,15	56,23	50,12	57,54	77,62	53,7
7a	GI_{50}	1,23	2,4	1,66	1,82	1,7	2,63	1,86	2,14	2	1,91
	TGI	6,92	6,92	3,31	4,27	3,72	7,59	4,17	5,62	6,17	5,13
	LC_{50}	100	33,11	6,76	15,85	9,33	33,88	10	18,62	16,98	18,62
7d	GI_{50}	1,66	1,82	1,51	1,35	1,58	2,14	1,58	1,48	1,62	1,62
	TGI	9,77	4,9	3,24	3,24	3,31	10,72	3,47	3,31	3,31	4,47

	LC_{50}	100	26,3	9,33	7,76	10,23	32,36	7,41	5,5	18,2	17,38
7f	GI_{50}	2,4	3,39	2,04	2,29	2,19	2,69	3,09	2,14	2,45	2,57
	TGI	11,22	14,13	4,68	5,89	5,25	8,91	8,51	5,37	6,92	7,59
	LC_{50}	100	45,71	11,22	28,84	19,5	44,67	39,81	28,18	37,15	33,11
7j	GI_{50}	2,69	9,33	4,37	4,68	7,24	6,46	7,08	5,89	5,37	5,89
	TGI	95,5	70,79	63,1	100	61,66	69,18	81,28	25,7	81,28	72,44
8b	GI_{50}	4,27	14,45	8,91	13,8	18,62	14,13	26,3	3,39	10	12,88
	TGI	-	56,23	5,23	67,61	85,11	93,33	74,13	41,69	64,57	70,79
8e	GI_{50}	3,16	2,57	2,04	3,16	2,14	3,16	2,34	2,57	3,09	2,63
	TGI	56,23	12,59	6,31	17,78	4,79	28,18	5,89	23,99	18,62	12,88
	LC_{50}	-	85,11	13,49	67,61	30,2	89,13	25,7	56,23	64,57	48,98
8k	GI_{50}	3,09	2,57	3,63	2,15	2,19	2,82	2,29	2,45	3,09	2,63
	TGI	83,18	14,79	7,41	9,33	11,48	29,51	17,38	22,39	29,51	18,2
	LC_{50}	-	52,48	31,62	-	51,29	69,18	-	-	-	67,61
8m	GI_{50}	2,51	6,76	3,31	8,51	6,03	6,61	6,31	2,95	3,98	5,13
	TGI	22,91	44,67	10,23	40,74	17,78	38,9	29,51	25,12	25,7	26,3
	LC_{50}	-	52,48	46,77	93,33	54,95	77,62	89,13	-	-	74,13
11n	GI_{50}	16,98	18,2	23,44	7,08	27,54	28,18	9,77	10,72	4,17	14,45
11o	GI_{50}	2,24	1,78	2	1,74	2,04	2,14	1,78	1,95	3,16	2,04
	TGI	6,17	4,79	4,68	4,07	4,9	4,69	4,47	3,39	6,31	4,9
	LC_{50}	89,13	24,55	11,75	18,2	12,88	12,59	14,79	7,94	21,88	18,62
11v	GI_{50}	1,2	2,19	1,78	1,82	2,34	2,45	1,95	1,82	24,55	2,04
	TGI	5,37	11,48	4,17	7,76	6,46	10,72	7,24	11,48	10	7,59
	LC_{50}	42,66	51,29	9,77	38,02	22,39	45,71	28,18	20,42	33,11	28,84
Vincristine sulfate [d]	GI_{50}	0,1	0,25	0,1	0,13	0,16	0,32	0,32	0,13	0,32	0,2
	TGI	15,85	15,85	3,98	6,31	7,94	19,95	19,95	6,31	7,94	10

[a] Dark red is used for the lowest values (highest activity), dark blue for the highest values (lowest activity). [b] Highest conc. = 100 μM, only modes showing a value <100 μM are reported. The compound exposure time was 48 h. [c] Mean graph midpoint: average value for all cell lines tested; i.e., mean GI_{50}. [d] Mean of two separate experiments.

drugs have already been developed to treat patients by targeting epigenetic changes. New research brings epigenetics and cancer together in studying molecular mechanisms and developing drug targets [18].

Increased gene expression is often associated with lysine acetylation at the N-terminal tails of histones H3 and H4 [19,20].

First, after 6 h of treatment of IGROV1 with molecule **5f**, we analyzed whether histone acetylation differed from the vehicle. The levels of H2/H3-Kac and H4-Kac were significantly higher in treated IGROV1 cells than in control cells. Notably, compound **5f** leads to a significant increase in acetylation of histones H2/H3 and H4 by 55.2% ± 8.97 and 68.5% ± 6.97, respectively. The distribution of global histone acetylation levels in IGROV1 is shown in Fig. 6A.

To test whether epigenetic modifications are related to changes in gene expression, Real Time PCR (RT-PCR) and Western blot analysis of the corresponding protein products were performed. The transcript levels of both genes involved in the control of the G0/G1 phase of the cell cycle, such as CCND1 (cyclin D1) and CDNK1 (p21), and those controlling adhesion, such as ITAG5 (α subunit of integrin β1) were specifically examined.

Cyclin D1 is a 36 kDa protein encoded by the CCND1 gene on chromosome 11q13 and is expressed in most normal human cells [21].

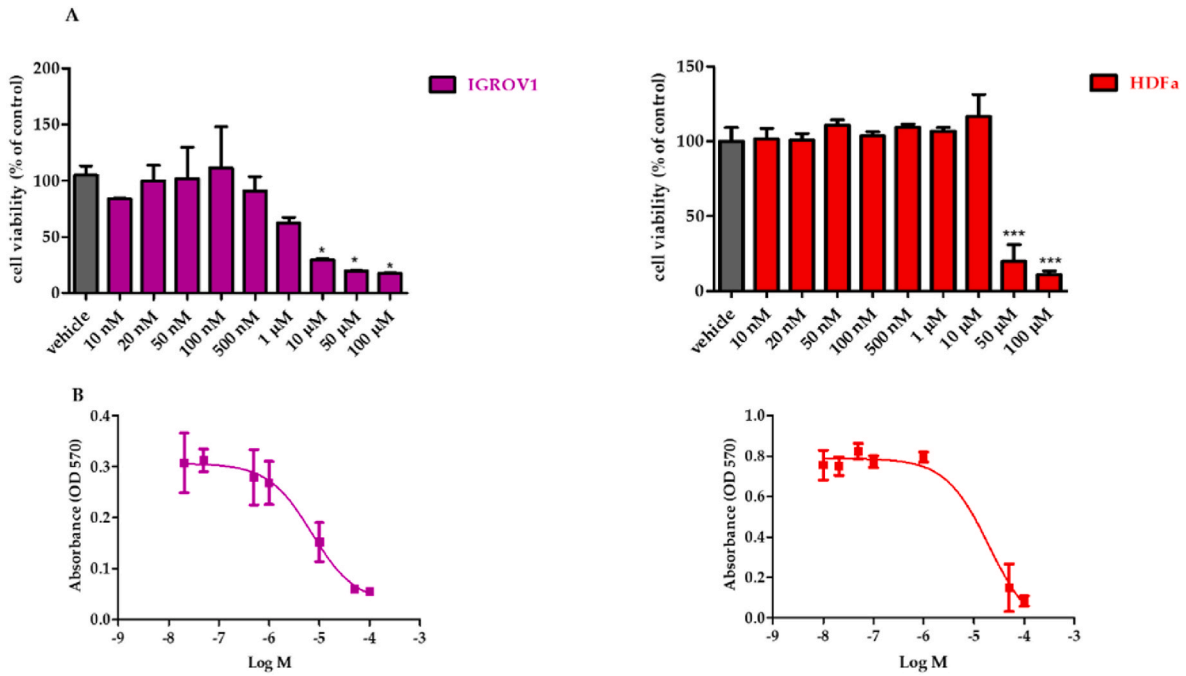

Fig. 1. Effect of **5f** on the viability of transformed and non-transformed human cells. A) IGROV1 and HDFa were incubated for 24 h with increasing concentrations of **5f** (from 0.01 to 100 μM). Viability was evaluated by MTT test. Black bars correspond to the control (vehicle). Results are expressed as means ± SD of three independent experiments. B) Dose-response curves are reported as the mean ± SD from three independent experiments (n = 3), each performed in triple.

Table 2
Cytotoxic effect expressed as IC_{50} μM.

Cell lines	IC_{50} (μM)	SI[a]
HDFa	21.93 ± 0.13	–
IGROV1	6.06 ± 0.01	3.46 ± 0.6

[a] SI=(IC_{50} for HDFa)/(IC_{50} for the cancer line).

In many cells, its expression is triggered very early by growth factors. Dysregulation of transcription, accumulation and ubiquitination of cyclin D1, or assembly and hyperactivation of the cyclin-dependent kinase CDK lead to uncontrolled cell growth. Therefore, cyclin D1 is considered as an oncogenic factor in various cancers such as breast cancer, lung cancer and melanoma [22].

p21 belongs to the Cip/Kip family of CDK inhibitors and inhibits cell cycle progression mainly by impairing cyclin D1/cdk4 and cyclin E/cdk2 activity [23].

Integrins, the family of heterodimeric cell surface receptors are found in most cells, both normal and tumor cells. These receptors are known to play important regulatory roles in both the processes of mechanical attachment of cells to the extracellular matrix an as well as in the processes that generate signals involved in various diseases, including autoimmune diseases, cardiovascular diseases, and malignancies [24,25]. Strategies aimed at blocking integrin-β1 signaling, particularly α5β1, have been shown to be effective in reducing tumor growth in preclinical models. Park et al. reported how a β1-integrin inhibitory antibody significantly impairs in vitro and in vivo growth of human breast cancer tumor cells [26]. Using volociximab, a monoclonal antibody that blocks function against α5β1-integrin, Bhaskar et al. showed that this drug can inhibit angiogenesis and prevent tumor growth [27,28].

Therefore, the transcript levels of CCND1, CDKN1A, and ITAG5 were analyzed using the cDNA of IGROV1 vehicle and **5f**-treated genes. Fig. 6B shows that treatment with **5f** 5 μM for 6 h significantly reduces the expression of the CCND1 ($p \leq 0.005$) and ITAG5 ($p \leq 0.005$) genes, resulting in a decrease in the corresponding protein products (Fig. 6C). In contrast, **5f** does not alter gene expression (Fig. 6B) or protein levels of p21 (data not shown).

The data show that compound **5f** causes greater quiescence in the G0/G1 phase of the cell cycle by a mechanism that results in decreased expression of cyclin D1, whereas p21 levels are not altered, suggesting that the p53-mediated cycle is not involved. In addition, the alpha-5 subunit of integrin β1 decreases, contributing not only to growth quiescence but more importantly to a decrease in migratory capacity.

2.2.6. *Induction of DNA damage in IGROV1 cells*

Cyclin D1 not only plays a role in cell cycle regulation, where it acts in conjunction with CDK4/6 or other partners such as transcription factors, chromatin-modifying enzymes, or cytosolic proteins, but also regulates a number of key processes involved in cancer development and maintenance. Among these processes is the response to DNA damage [29,30].

Cyclin D1 has recently been investigated as an important protein in DNA damage repair mechanisms, particularly in homologous recombination-directed repair (HDR) [30]. Cyclin D1 is recruited by BRCA2 to damaged foci and enhances the binding of RAD51 to BRCA2, as cyclin D1 prevents the inhibitory phosphorylation of BRCA2 at serine 3291. In addition, cyclin D1 is essential for the upregulation of the RAD51 gene in the event of a double-strand break (DSB) [31].

It has also been observed that knockdown of CCND1 significantly increases the sensitivity of cancer cells to ionizing radiation (IR) and to DNA-damaging drugs such as topoisomerase inhibitors. Re-expression of cyclin D1 in these cells restores radiosensitivity. Moreover, treatment with a specific inhibitor of CDK4/6 kinase has no effect on the radiosensitivity of cancer cells; for this reason, cyclin D1 may play a kinase-independent function in DNA repair. It has been found that radiation causes comparable amounts of DNA damage in control and cyclin D1-depleted cells, but that more unrepaired DNA is present in cyclin D1-depleted cells 16 h after irradiation. Radiosensitization induced by silencing of cyclin D1 depends on increased accumulation of double-strand breaks (DSBs) [30,31].

Therefore, IGROV1 were treated with compound **5f** 5 μM for 24 h to decrease cyclin D1 expression and then exposed to UV irradiation to

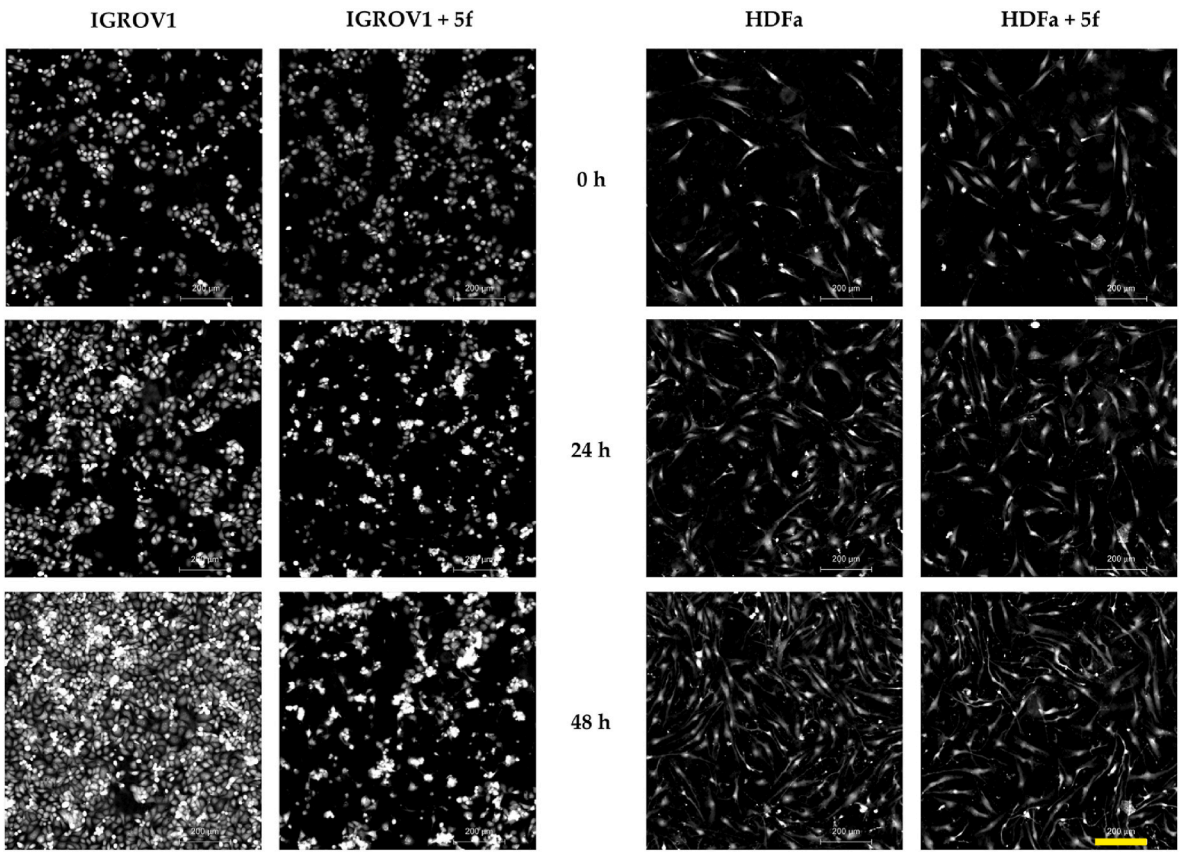

Fig. 2. Quantitative phase images. Representative images of IGROV1 and HDFa cells after 0, 24, and 48 h of treatment with 5 μM **5f**. Images of untreated cells are shown for comparison. Scale bar: 200 μm.

induce DBS damage.

Quantification of the γH2AX marker was determined after 24 h of treatment with 5 μM **5f** and after 6 h of UV irradiation of cells treated with **5f**.

The analysis shows a strong increase in DSB marker in irradiated cells compared to control cells. In addition, UV irradiation significantly increases H2AX phosphorylation in cells treated with **5f** for 24 h compared to vehicle cells and to vehicle exposed to UV (+35% ± 20), as shown in Fig. 7A.

Subsequently, qRT-PCR analysis of CCND1 and RAD51 genes has been performed to examine cyclin D1 protein-dependent RAD51 expression (Fig. 7B). These results underscore the downregulation of CCND1 in both UV-irradiated and **5f**-treated cells. The **5f**-UV sample shows a decrease in cyclin D1 expression compared to the control. RAD51 mRNA analysis shows upregulation induced by irradiation, which is not present in cells treated with **5f** and then irradiated.

The Western blot of cyclin D1 and RAD51 has been then analyzed and quantified in the vehicle, UV-irradiated, **5f**-treated, and irradiated cells after **5f** treatment. Fig. 7C shows that the amount of cyclin D1 decreases in all treated cells and RAD51 increases in UV-irradiated cells but not in cells treated with **5f** for 24 h and then irradiated.

To test whether cyclin D1 depletion could play an active role in mediating the DNA damage response, a siRNA silencing experiment for the gene encoding cyclin D1 protein has been performed.

First, the silencing level was determined by quantifying the cyclin D1 protein 48 h after siRNA treatment. Fig. 8A shows that the siRNA concentration of 10 nM used for subsequent analysis results in almost complete silencing.

Fig. 8B shows how cyclin D1 concentration decreases by 91.1 ± 1.3 and 91.7% ± 2.1 in control and silencing cells irradiated with UV, respectively. After UV irradiation, phosphorylation of histone H2AX increases by 39.1 ± 1.9 and 78.5% ± 1.4 in both control and siRNA cells, respectively (Fig. 8C). qRT-PCR analyses of CCND1 (Fig. 8D) and RAD51 genes have been performed to examine cyclin D1 protein-dependent RAD51 expression in all samples. Irradiation results in downregulation of CCND1 and upregulation of RAD51 genes. Surprisingly, silenced cells show downregulation of CCND1 but no upregulation of RAD51 in response to UV irradiation. In contrast, the scramble sample behaves like the control cells.

3. Conclusions

In this work, the design and synthesis of new bis-indolinone derivatives were reported. In an initial screening, a series of novel Knoevenagel adducts was submitted to the National Cancer Institute for evaluation of antitumor activity in human cell lines. After initial screening, compound **5f** was selected to evaluate its biological activity in IGROV1 and HDFa. A first important result was provided by the MTT assay, which showed that **5f** was more potent in IGROV1 (IC_{50} 6.06 μM ± 0.01) than in HDFa (21.93 μM ± 0.13), indicating a lower cytotoxicity toward normal cells. These results are consistent with those of the QPI analysis showing that treatment with **5f** in IGROV1 leads to more impressive biological effects by permanently altering important cellular parameters such as cell count, cell confluence, and DT. It also alters motility, suggesting that these cells lose their migratory ability. The antiproliferative effect is characterized by a growth arrest in the G0/G1 phase, leading to a decrease in the population in S and G2/M. This arrest is characterized by an increase in histone acetylation leading to altered expression of the CCND1 and ITAG5 genes, which contributes not only to growth arrest but also to loss of migratory ability. Cyclin D1 not only plays an important role in regulating the transition of the cell cycle from G1 to S phase, but also plays a non-kinase-dependent role in DNA repair

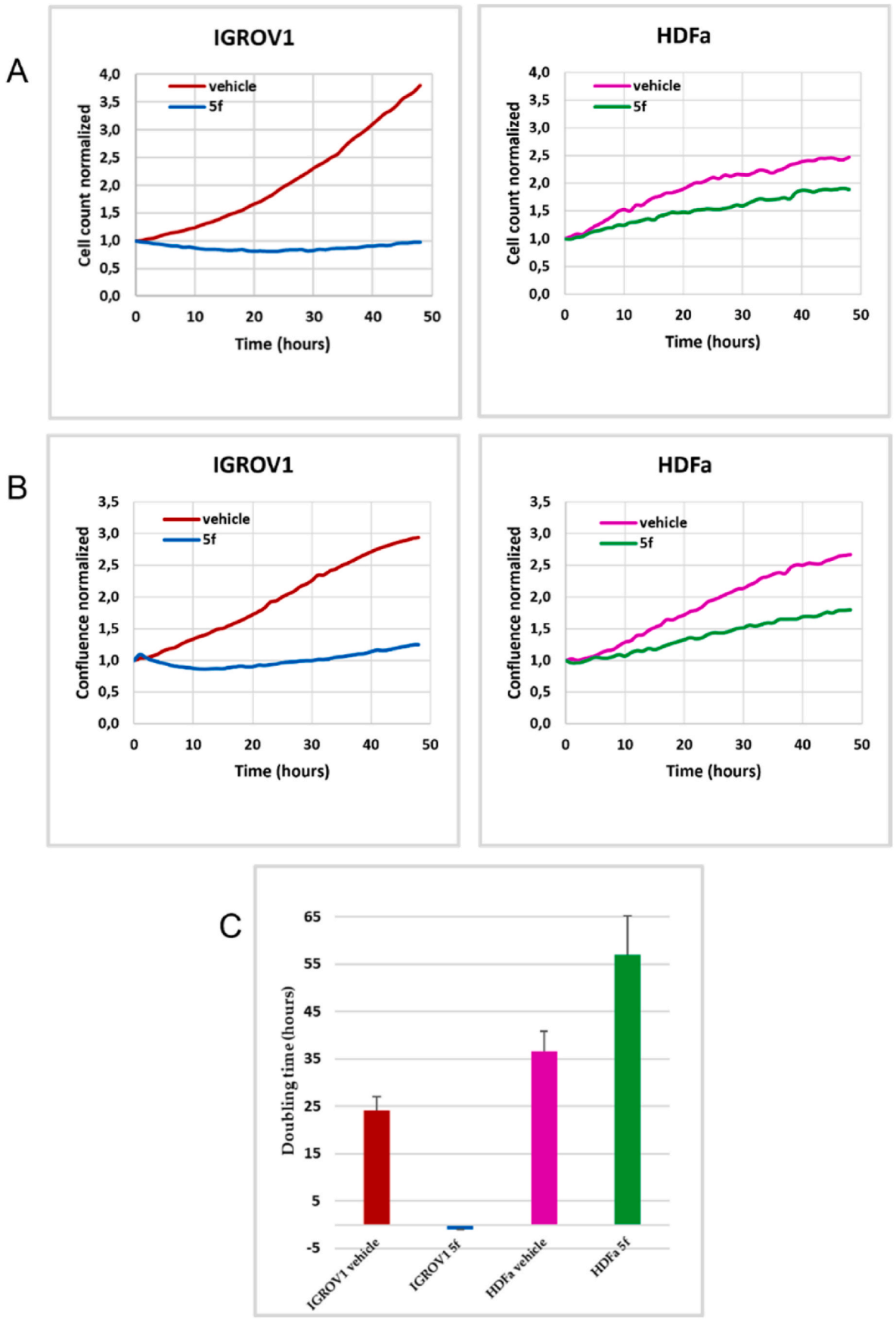

Fig. 3. Effect of **5f** treatment on cell proliferation. Cell count, cell confluence, cell doubling time for IGROV1 (A, C) and HDFa (B, D). Cells were treated (or not) with 5 μM **5f** for 24 or 48 h. Cell count and confluence were normalized on the start of experiment.

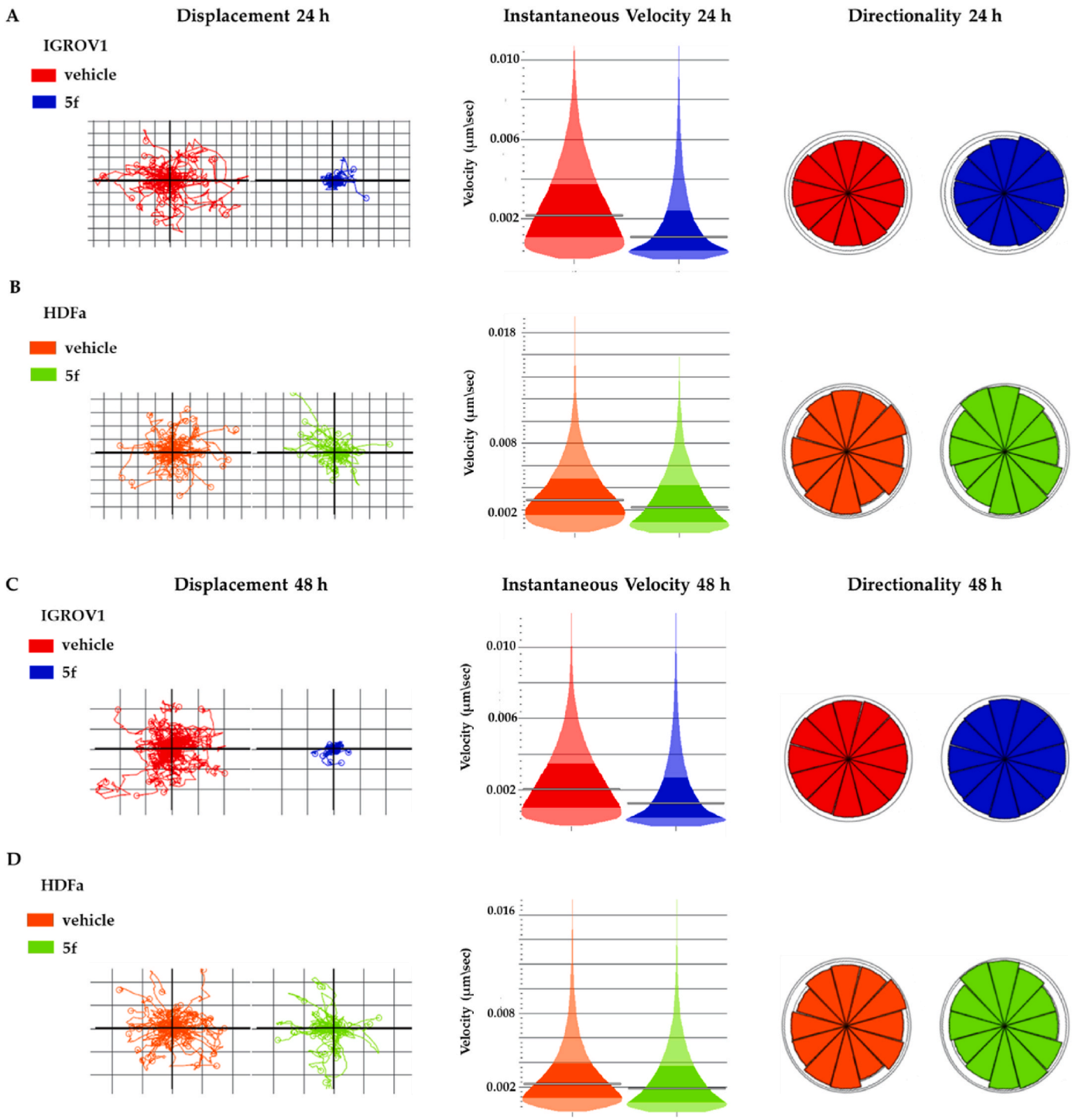

Fig. 4. Analysis of cellular motility. Displacement, instantaneous velocity and directionality of IGROV1 (A, C), and HDFa (B, D) cells after 24 and 48 h of treatment with 5 μM **5f**, respectively.

by affecting it through interaction with RAD51 [30]. Reducing cyclin D1 levels in human cancer cells impairs RAD51 recruitment to damaged DNA, which prevents DNA repair and increases cell sensitivity to radiation in vitro and in vivo [46,47]. Consistent with this knowledge, we have shown that 24 h treatment with **5f** increases radiosensitivity by causing greater DNA damage, as suggested by increased histone H2AX phosphorylation and decreased RAD51 protein levels, in a manner comparable to cyclin D1 gene silencing. **5f** is undoubtedly a promising compound that could be used in a combined treatment of a drug leading to depletion of cyclin D1 and a DNA damage inducer, such as irradiation, thereby increasing the possibility of targeting ovarian tumors, especially in cases of chemo- and radiation-resistance. Ovarian cancer ranks among the most prevalent gynecological malignancies and significantly contributes to morbidity and mortality in women worldwide due to high mortality rate, propensity for late-stage diagnosis, and a notable tendency for recurrence even after successful initial treatment. The unique challenges posed by ovarian cancer emphasize the critical need for continuous research and the development of innovative therapies to minimize collateral effects and improve outcomes for affected individuals. In this scenario, the identification of a molecule that

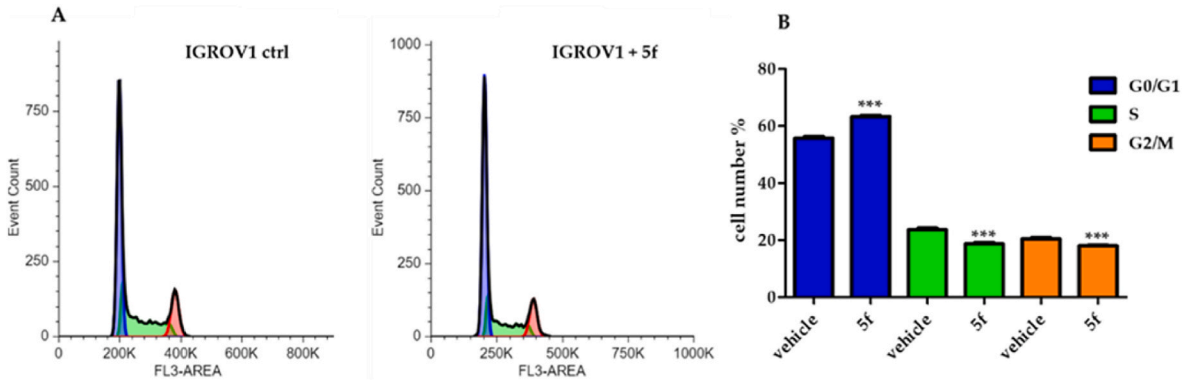

Fig. 5. Cell cycle analysis. A) IGROV1 cells were treated with 5 μM 5f for 24 h and then analyzed by flow cytometry. The histogram shows the cell cycle profile of a representative experiment. B) Percentage distribution of cells in the different cell cycle phases. Error bars are standard deviations. Significant differences are indicated by ***$p \leq 0.005$.

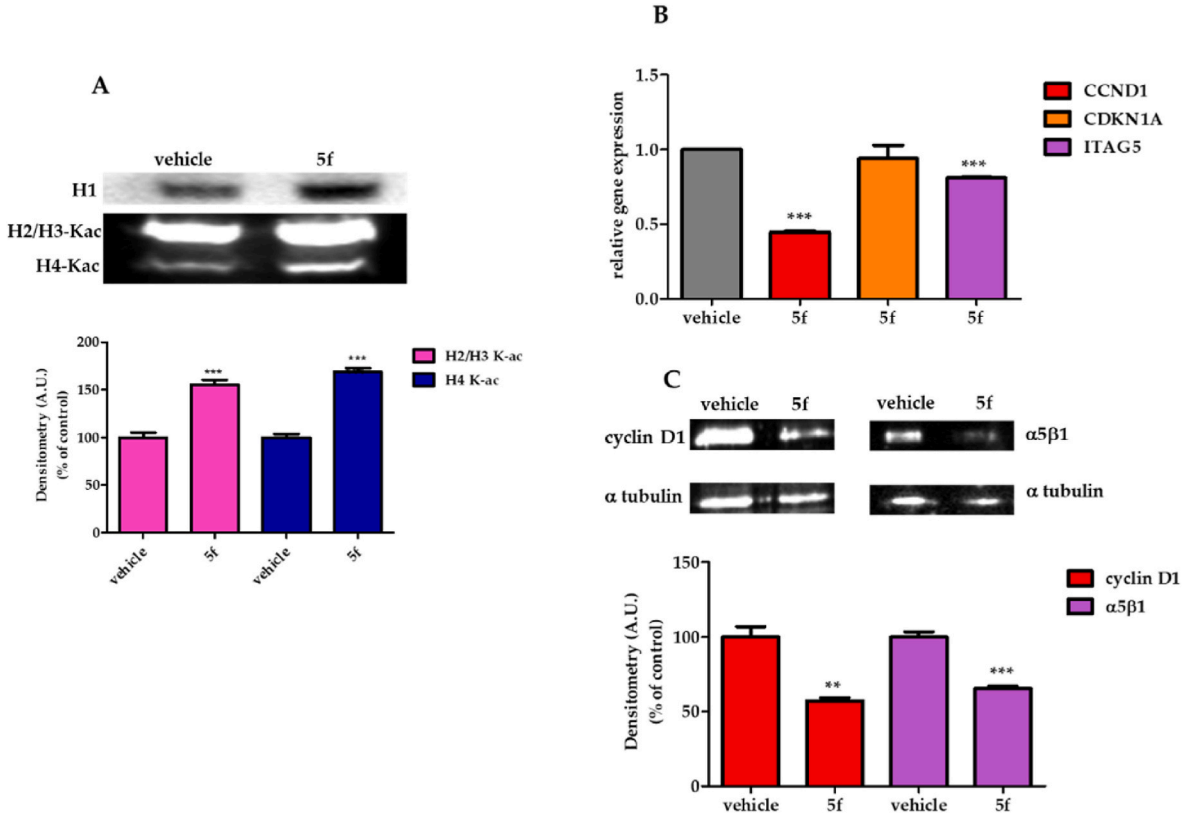

Fig. 6. **5f** modified histone acetylation, gene and protein expression. A) Effects of **5f** on H2/H3 and H4 acetylation of IGROV1 cells. (Above). Representative Western blot image of acetylated histones. (Below). Relative quantification of H2/H3-acetylated histones in IGROV1 vehicle cells and those exposed to compound **5f** for 6 h. Densitometric units (A.U.) were normalized to H1 histone. Results are expressed as means ± SD of three independent experiments and were compared with vehicle, which are considered 100%. (***$p \leq 0.005$). B) Normalized gene expression for CCND1, CDKN1A and ITAG5 analyzed by RT-PCR. Data are expressed as the mean of relative expression (fold change) between treatment **5f** and vehicle sample. Significant differences are indicated by ***$p \leq 0.005$. C) (Above). Western blot analysis of cyclin D1 and α5β1. (Below). Relative quantification of the proteins. Arbitrary units (A.U.) of densitometry are normalized by α-tubulin. Results are given as means ± SD of three independent experiments and are compared with vehicle, which are considered 100%. Significant differences are indicated by **$p \leq 0.01$ and ***$p \leq 0.005$.

selectively arrests ovarian cancer cells proliferation, while sparing the healthy ones, and increases radiosensitivity, might represent a significant breakthrough in the field of ovarian cancer treatment and compound **5f** certainly represents a valuable starting point for this goal. As a future perspective, the mechanism of action by which **5f** leads to the downregulation of cyclin D1 will be investigated.

4. Material and methods

4.1. Chemistry

Melting points were determined in open glass capillaries, using a Büchi apparatus and are uncorrected. Elemental analyses were within ±0.4% of the theoretical values. Bakerflex plates (silica gel IB2–F) were used for TLC: the eluent was petroleum ether/acetone in various

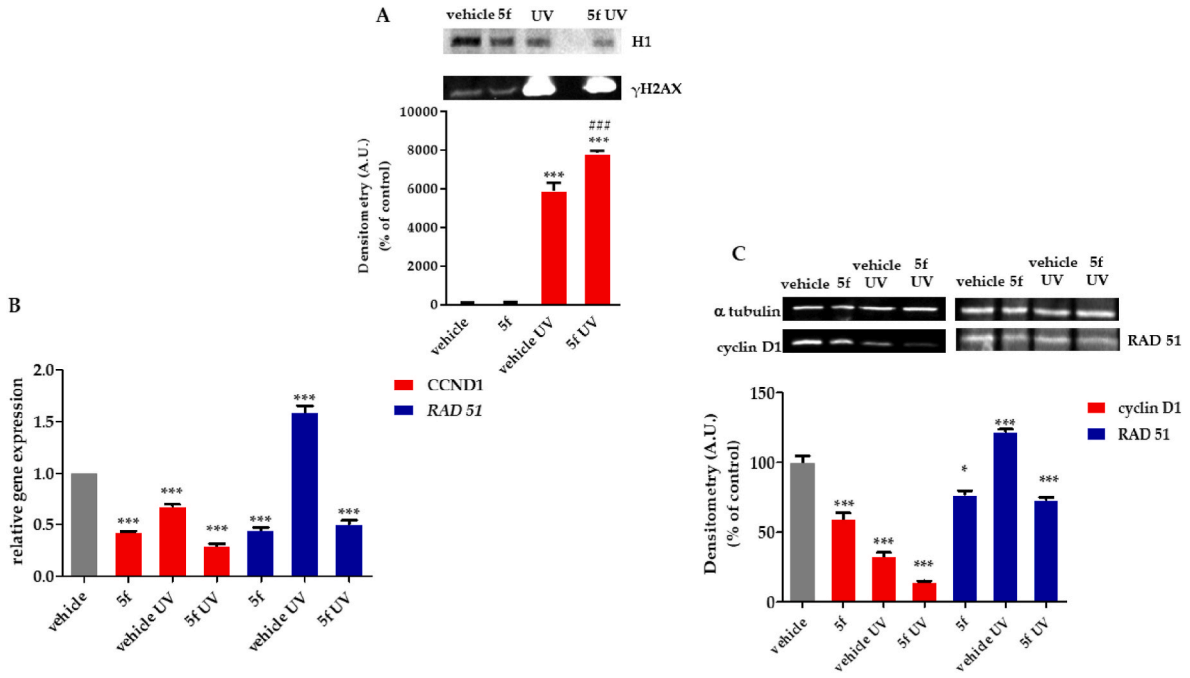

Fig. 7. **5f** induces DNA damage in IGROV1. A) (Above). Representative image of Western blot. (Below). Quantification of γH2AX marker in IGROV1 cells. Densitometric units (A.U.) are normalized to H1 histone. Results are expressed as means ± SD of three independent experiments and are compared to vehicle (***p ≤ 0.005), or **5f** UV to vehicle UV (###p ≤ 0.005). B) Normalized gene expression for CCND1 and RAD 51 analyzed by RT-PCR. Data are expressed as the mean of relative expression (fold change) between the treatment and control samples. Significant differences are indicated by ***p ≤ 0.005. (C) (Above). Representative image of Western blot of cyclin D1 and RAD 51. (Below). Relative quantification of the proteins. Densitometric arbitrary units (A.U.) are normalized by α-tubulin. Results are given as means ± SD of three independent experiments and are compared with controls, which are considered 100%. Significant differences are indicated by * p ≤ 0.05, and ***p ≤ 0.005.

proportions. The IR spectra were recorded in nujol on a Nicolet Avatar 320 E.S.P. ν_{max} is expressed in cm^{-1}. IR bands intensities are referred as strong (s), medium (m) and weak (w). ^1H NMR and ^{13}C NMR spectra were recorded in $(CD_3)_2SO$ on a Varian MR 400 MHz (ATB PFG probe, Crawley, United Kingdom); the chemical shift (referenced to solvent signal) is expressed in δ (ppm) and J in Hz; abbreviations: ar = aromatic, bz = benzyl, ind = indole, phen = phenanthroline. UHPLC−MS analyses were run on a Waters ACQUITY ARC UHPLC/MS system, consisting of a QDa mass spectrometer equipped with an electrospray ionization interface and a 2489 UV/Vis detector at wavelengths (λ) 254 nm and 365 nm. High-resolution mass spectrometry (HRMS) data were analyzed by flow injection, utilizing electrospray ionization (ESI) on a Waters Xevo G2-XS QTOF (Milford, MA, United States) instrument in the positive mode.

Compounds were named relying on the naming algorithm developed by CambridgeSoft Corporation (PerkinElmer, Milan, Italy) and used in Chem-BioDraw Ultra 14.0 (PerkinElmer, Milan, Italy). ^1H NMR spectra of the seventeen compounds selected for the NCI full 5-concentration assay, ^{13}C NMR, and HRMS spectra of compound **5f** are reported as Supplementary Materials. All solvents and reagents, unless otherwise stated, were supplied by Aldrich Chemical Co. Ltd. (Milan, Italy) and were used without further purification.

4-fluoroindolin-2-one **1a** [32], 4,5,6-triethylindolin-2-one **1b** [33], 4,7-dichloroindolin-2-one **1c** [34], 5-fluoroindolin-2-one **1d** [35], 5-methoxy-1-methylindolin-2-one **1e** [36], 6-chloroindolin-2-one **1f**, 1-benzylindolin-2-one **1g** [37], 5-hydroxy-6-methylindolin-2-one **1h** [38], 1-(4-chlorobenzyl)indolin-2-one **1i** [39], 4,7-dimethoxyindolin-2-one **1j** [40], 5-chloroindolin-2-one **1k**, 5-chloro-1-methylindolin-2-one **1l** [41], 5-methoxy-6-methylindolin-2-one **1m** [42], 4-tert-butyl-2,6-diformylphenol **2**, benzene-1,3-dicarbaldehyde **3**, 1,10-phenanthroline-2,9-dicarbaldehyde **4**, and 1,7-dimethyl-5,7-dihydropyrrolo [3,2-f]indole-2,6(1H,3H)-dione **10** [43] are commercially available or have been prepared as described in the literature.

*4.1.1. Synthesis of compounds **5a–i, 6, 7a, d, f-h, i-j, m, 8b, e, g, i–m, 11n-x***

Four different methods were employed.

*4.1.1.1. Method 1 (compounds **5a–b, d–i, 6, 7h-i, x, 8b, e, g, i–m, 11n-x**).*

The proper compound **1**(10 mmol) was dissolved in methanol (100 mL) and treated with the appropriate aldehyde **2**, **3** or **4** (5 mmol) and piperidine (2 mL). The reaction mixture was refluxed for 3–8 h (according to a TLC test), cooled and, if necessary, concentrated at reduced pressure or treated with water (100 mL). The yellow to orange precipitate thus formed was collected by filtration. The compounds were subjected to biological tests after crystallization from ethanol. The compound **5h** was subjected to biological tests after purification by column chromatography; in the course of the purification, the monosubstituted derivative **6** was also isolated.

Since compounds **11** have an indolinone central core, the same procedure was used for their synthesis, but the stoichiometric ratios have been inverted: 5 mmol of the indolinone **10** and 10 mmol of the appropriate aldehyde **9**.

(3E,3′E)-3,3′-((5-(tert-butyl)-2-hydroxy-1,3-phenylene)bis(methaneylylidene))bis(4-fluoroindolin-2-one) **5a**, Brownish solid; Yield 45%; m.p.: 258–260 °C; IR (Nujol) ν_{max}: 3151, 1710 (s), 1617 (s), 1506 (m), 1153 (w) cm^{-1}; ^1H NMR (DMSO–d_6): δ 1.28 (s, 9H, $3CH_3$), 6.69 (dd, J = 9.2, 4.6, 2H), 6.69 (d, J = 9.2, 2H, ind), 7.47 (m, 2H, ind), 7.72 (s, 4H, 2CH+2ar), 9.81 (broad s, 1H, OH), 10.75 (s, 2H, 2NH); MS (ES) *m/z*: 473.14 (M + H); Anal. Calcd for $C_{28}H_{22}F_2N_2O_3$ (MW: 472.49): C, 71.18; H, 4.69; N, 5.93; Found C, 71.21; H, 4.67; N, 5.92.

(3E,3′Z)-3,3′-((5-(tert-butyl)-2-hydroxy-1,3-phenylene)bis(methaneylylidene))bis(4,5,6-trimethoxyindolin-2-one) **5b**, Red solid; Yield 24%; m.p.: 246–249 °C; IR (Nujol) ν_{max}: 3400–3200 (m), 1685 (m), 1624 (s), 1124 (m) cm^{-1}; ^1H NMR (DMSO–d_6): δ 1.26 (s, 9H, $3CH_3$), 3.01 (s, 3H, OCH_3), 3.63 (s, 3H, OCH_3), 3.72 (s, 3H, OCH_3), 3.82 (s, 6H, $2OCH_3$), 3.94 (s, 3H, OCH_3), 6.32 (s, 1H, ind), 6.36 (s, 1H, ind), 7.14 (d, J = 1.6,

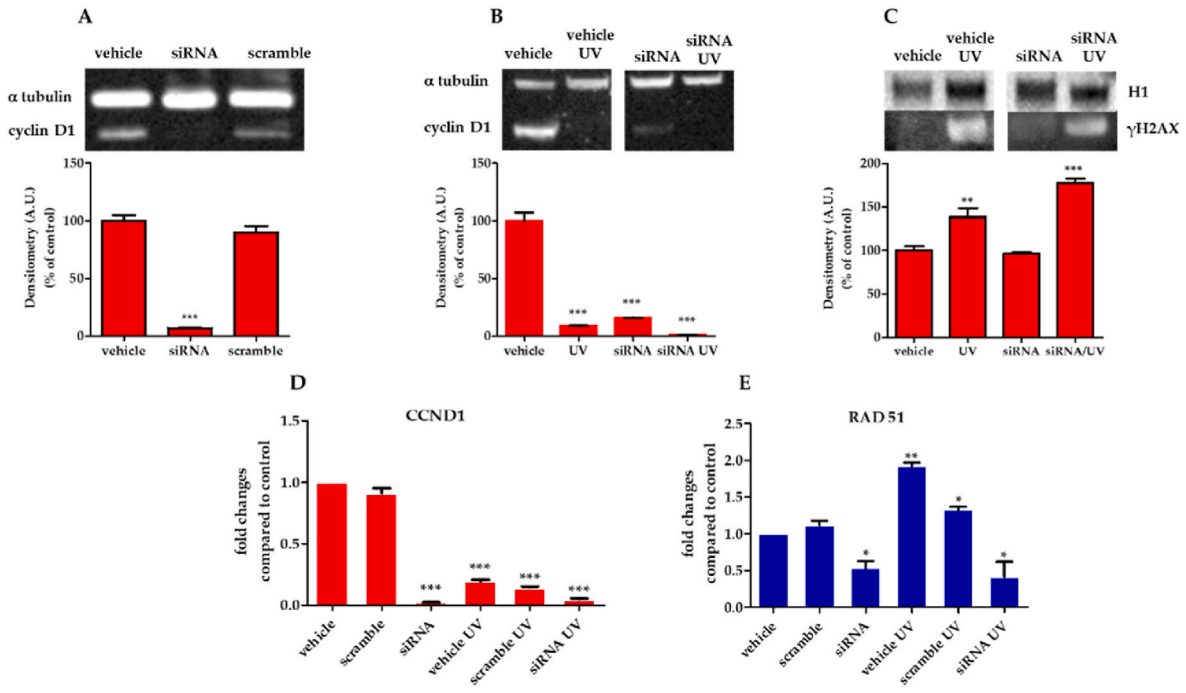

Fig. 8. Increased radiosensitivity of tumors with reduced cyclin D1 levels. A) (Above). Western blot. Representative image of proteins extracted from vehicle, siRNA, and scramble. (Below). Densitometric units (A.U.) were normalized by α-tubulin. Results are given as means ± SD of three independent experiments and are compared with vehicle (control), which is considered 100%. Significant differences are indicated by ***p ≤ 0.005. B) (Above). Western blot. Representative image of proteins extracted from vehicle, vehicle UV, siRNA, and siRNA UV. (Below). Densitometric units (A.U.) were normalized by α-tubulin. Results are given as means ± SD of three independent experiments and are compared with vehicle. Significant differences are indicated by ***p ≤ 0.005 versus vehicle. C) Quantification of the γH2AX marker in IGROV1 cells by Western blot. (Above). Representative image of histones extracted from vehicle, vehicle UV, siRNA, and siRNA UV. (Below). Densitometric units (A.U.) are normalized to H1 histone. Results are expressed as means ± SD of three independent experiments and compared with controls as 100% (**p ≤ 0.05, ***p ≤ 0.005 vs. vehicle). D, E) $2^{-\Delta\Delta CT}$ levels of CCND1 and RAD51 gene expression in IGROV1 cells. RNA extracted from vehicle, scramble, siRNA and vehicle UV, scramble UV and siRNA UV. (***p ≤ 0.005 vs vehicle). The conditions and times of UV treatment are listed in the section "Materials and methods".

1H, ar), 7.71 (s, 1H, CH), 8.23 (s, 1H, CH), 8.41 (d, $J = 1.6$, 1H, ar), 9.53 (s, 1H, OH), 10.44 (s, 1H, NH), 10.50 (s, 1H, NH); MS (ES) *m/z*: 617.24 (M + H); Anal. Calcd for $C_{34}H_{36}N_2O_9$ (MW: 616.67): C, 66.22; H, 5.88; N, 4.54; Found C, 66.20; H, 5.90; N, 4.55.

(3E,3′E)-3,3′-((5-(tert-butyl)-2-hydroxy-1,3-phenylene)bis(methaneylylidene))bis(5-fluoroindolin-2-one) **5d**, Orange solid; Yield 40%; m.p.: 272–274 °C; IR (Nujol) ν_{max}: 3595–3391 (w), 3159 (m), 1707 (s), 1613 (s) cm^{-1}; ^1H NMR (DMSO–d_6): δ 1.31 (s, 9H, $3CH_3$), 6.87 (dd, $J =$ 8.6, 4.6, 2H, ind), 7.08 (td, $J = 9.4$, 2.6, 2H, ind), 7.19 (dd, $J = 9.4$, 2.6, 2H, ind), 7.76 (s, 2H, ar), 7.82 (s, 2H, 2CH), 10.10 (broad s, 1H, OH), 10.62 (s, 2H, 2NH); MS (ES) *m/z*: 473.15 (M + H); Anal. Calcd for $C_{28}H_{22}F_2N_2O_3$ (MW: 472.49): C, 71.18; H, 4.69; N, 5.93; Found C, 71.18; H, 4.71; N, 5.90.

(3E,3′E)-3,3′-((5-(tert-butyl)-2-hydroxy-1,3-phenylene)bis(methaneylylidene))bis(5-methoxy-1-methylindolin-2-one) **5e**, Red solid; Yield 40%; m.p.: 255–260 °C; IR (Nujol) ν_{max}: 1708 (s), 1679 (s), 1592 (s), 1216 (s), 1031 (m) cm^{-1}; ^1H NMR (DMSO–d_6): δ 1.20 (s, 9H, $3CH_3$), 3.20 (s, 6H, $2OCH_3$), 3.61 (s, 6H, $2NCH_3$), 6.93 (dd, $J = 8.4$, 2.4, 2H, ind-6), 6.97 (d, $J = 8.4$, 2H, ind-7), 7.03 (d, $J = 2.4$, 2H, ind-4), 7.72 (s, 2H, ar), 7.80 (s, 2H, 2CH), 9.93 (s, 1H, OH); MS (ES) *m/z*: 525.28 (M + H); Anal. Calcd for $C_{32}H_{32}N_2O_5$ (MW: 524.62): C, 73.26; H, 6.15; N, 5.34; Found C, 73.24; H, 6.14; N, 5.37.

(3E,3′E)-3,3′-((5-(tert-butyl)-2-hydroxy-1,3-phenylene)bis(methaneylylidene))bis(6-chloroindolin-2-one) **5f,** Brown solid; Yield 62%; m.p.: 250–252 °C; IR (Nujol) ν_{max}: 3600–3100 (m), 1709 (s), 1608 (s), 1324 (m) cm^{-1}; ^1H NMR (DMSO–d_6): δ 1.28 (s, 9H, $3CH_3$), 6.90 (d, $J =$ 2.1, 2H, ind-7), 6.93 (dd, $J = 8.2$, 2.1, 2H, ind-5), 7.44 (d, $J = 8.2$, 2H, ind-4), 7.73 (s, 2H, ar), 7.78 (s, 2H, 2CH), 9.95 (broad s, 1H, OH), 10.75 (s, 2H, 2NH); ^{13}C NMR (DMSO-d_6): δ 31.06, 34.30, 110.08, 120.17, 120.67, 123.00, 123.59, 128.91, 133.33, 133.86, 143.96, 144.12, 168.64; HRMS: *m/z* calculated for $C_{28}H_{23}Cl_2N_2O_3$ $[M + H]^+$: 505.1086 Found: 505.1075; Anal. Calcd for $C_{28}H_{22}Cl_2N_2O_3$ (MW: 505.40): C, 66.54; H, 4.39; N, 5.54; Found C, 66.53; H, 4.40; N, 5.52.

(3E,3′E)-3,3′-((5-(tert-butyl)-2-hydroxy-1,3-phenylene)bis(methaneylylidene))bis(1-benzylindolin-2-one) **5g**, Yellow solid; Yield 54%; m.p.: 225–228 °C; IR (Nujol) ν_{max}: 1698 (s), 1679 (s), 1607 (s), 1262 (m), 1197 (m) cm^{-1}; ^1H NMR (DMSO–d_6): δ 1.29 (s, 9H, $3CH_3$), 5.01 (s, 4H, $2CH_2$), 6.91 (t, $J = 7.8$, 2H, ind), 7.00 (d, $J = 7.8$, 2H, ind), 7.24 (t, $J =$ 7.8, 2H, ind), 7.28 (m, 2H, bz), 7.36 (m, 8H, bz), 7.55 (d, $J = 7.8$, 2H, ind), 7.81 (s, 2H, ar), 7.91 (s, 2H, 2CH), 10.05 (broad s, 1H, OH); MS (ES) *m/z*: 617.29 (M + H); Anal. Calcd for $C_{42}H_{36}N_2O_3$ (MW: 616.76): C, 81.79; H, 5.88; N, 4.54; Found C, 81.77; H, 5.87; N, 4.58.

(3E,3′E)-3,3′-((5-(tert-butyl)-2-hydroxy-1,3-phenylene)bis(methaneylylidene))bis(5-hydroxy-6-methylindolin-2-one) **5h**, Brown solid; Yield 18%; m.p.: 296–298 °C; IR (Nujol) ν_{max}: 3500–3100 (m), 1690 (s), 1619 (s), 1178 (m) cm^{-1}; ^1H NMR (DMSO–d_6): δ 1.31 (s, 9H, $3CH_3$), 2.12 (s, 6H, $2CH_3$), 6.59 (s, 2H, ind-7), 7.01 (s, 2H, ind-4), 7.59 (s, 2H, ar), 7.02 (s, 2H, 2CH), 8.62 (s, 2H, 2OH), 9.74 (s, 1H, OH), 10.21 (s, 2H, 2NH); MS (ES) *m/z*: 497.21 (M + H); Anal. Calcd for $C_{30}H_{28}N_2O_5$ (MW: 496.56): C, 72.56; H, 5.68; N, 5.64; Found C, 72.54; H, 5.67; N, 5.67.

(3E,3′E)-3,3′-((5-(tert-butyl)-2-hydroxy-1,3-phenylene)bis(methaneylylidene))bis(1-(4-chlorobenzyl)indolin-2-one) **5i**, Yellow solid; Yield 33%; m.p.: 248–250 °C; IR (Nujol) ν_{max}: 1690 (s), 1676 (s), 1606 (s), 1221 (m), 1193 (m) cm^{-1}; ^1H NMR (DMSO–d_6): δ 1.29 (s, 9H, $3CH_3$), 5.01 (s, 4H, $2CH_2$), 6.92 (t, $J = 7.6$, 2H, ind), 7.01 (d, $J = 7.6$, 2H, ind), 7.26 (t, $J = 7.6$, 2H, ind), 7.40 (m, 8H, bz), 7.55 (d, $J = 7.6$, 2H, ind), 7.81 (s, 2H, ar), 7.91 (s, 2H, 2CH), 10.06 (broad s, 1H, OH); MS (ES) *m/z*: 685.20 (M + H); Anal. Calcd for $C_{42}H_{34}Cl_2N_2O_3$ (MW: 685.65): C, 73.57; H, 5.00; N, 4.09; Found C, 73.60; H, 5.00; N, 4.06.

(E)-5-(tert-butyl)-2-hydroxy-3-((5-hydroxy-6-methyl-2-oxoindolin-3-ylidene)methyl)benzaldehyde **6,** Dark red solid; Yield 56%; m.p.: 252–254 °C; IR (Nujol) ν_{max}: 3403 (m), 1679 (s), 1637 (s), 1217 (w),

1186 (w) cm^{-1}; ^1H NMR (DMSO–d_6): δ 1.32 (s, 9H, $3CH_3$), 2.10 (s, 3H, CH_3), 6.59 (s, 1H, ind), 6.83 (s, 1H, ind, 7.49 (s, 1H, CH), 7.91 (d, J = 2.4, 1H, ar), 7.94 (d, J = 2.4, 1H, ar), 8.64 (s, 1H, OH), 10.17 (s, 1H, CHO), 10.23 (s, 1H, OH), 11.04 (s, 1H, NH); MS (ES) *m/z*: 352.14 (M + H); Anal. Calcd for $C_{21}H_{21}NO_4$ (MW: 351.40): C, 71.78; H, 6.02; N, 3.99; Found C, 71.75; H, 6.05; N, 3.98.

(3E,3′E)-3,3′-(1,3-phenylenebis(methaneylylidene))bis(5-hydroxy-6-methylindolin-2-one) **7h**, Red solid; Yield 10%; m.p.: 300–302 °C; IR (Nujol) ν_{max}: 3334 (m), 3180 (m), 1700 (s), 1190 (s), 1078 (s) cm^{-1}; ^1H NMR (DMSO–d_6): δ 2.08 (s, 6H, $2CH_3$), 6.59 (s, 2H, ind), 7.10 (s, 2H, ind), 7.55 (s, 2H, 2CH), 7.65 (t, J = 7.7, 1H, ar), 7.77 (d, J = 7.7, 2H, ar), 7.88 (s, 1H, ar), 8.90 (s, 2H, 2OH), 10.24 (s, 2H, 2NH); MS (ES) *m/z*: 425.14 (M + H); Anal. Calcd for $C_{26}H_{20}N_2O_4$ (MW: 424.46): C, 73.57; H, 4.75; N, 6.60; Found C, 73.54; H, 4.76; N, 6.62.

(3E,3′E)-3,3′-(1,3-phenylenebis(methaneylylidene))bis(1-(4-chlorobenzyl)indolin-2-one) **7i**, Yellow solid; Yield 37%; m.p.: 278–282 °C; IR (Nujol) ν_{max}: 1703 (s), 1598 (s), 1168 (m), 1096 (m), 1020 (w) cm^{-1}; ^1H NMR (DMSO–d_6): δ 4.96 (s, 4H, $2CH_2$), 6.86 (t, J = 7.7, 2H, ind), 6.96 (d, J = 7.7, 2H, ind), 7.22 (t, J = 7.7, 2H, ind), 7.36 (m, 9H, 8bz + ar), 7.50 (d, J = 7.7, 2H, ind), 7.68 (t, J = 7.8, 1H, ar), 7.82 (m, 3H, 2CH + ar), 7.96 (s, 1H, ar); MS (ES) *m/z*: 613.16 (M + H); Anal. Calcd for $C_{38}H_{26}Cl_2N_2O_2$ (MW: 613.54): C, 74.39; H, 4.27; N, 4.57; Found C, 74.40; H, 4.25; N, 4.59.

(3E,3′E)-3,3′-(1,3-phenylenebis(methaneylylidene))bis(5-methoxy-6-methylindolin-2-one) **7 m**, Dark red solid; Yield 32%; m.p.: 263–265 °C; IR (Nujol) ν_{max}: 3152 (m), 1706 (s), 1610 (m), 1207 (m), 1092 (w) cm^{-1}; ^1H NMR (DMSO–d_6): δ 2.11 (s, 6H, $2CH_3$), 3.43 (s, 6H, $2OCH_3$), 6.68 (s, 2H, ind), 7.03 (s, 2H, ind), 7.59 (s, 2H, 2CH), 7.70 (t, J = 7.7, 1H, ar), 7.82 (d, J = 7.7, 2H, ar), 8.05 (s, 1H, ar), 10.35 (s, 2H, 2NH); MS (ES) *m/z*: 453.19 (M + H); Anal. Calcd for $C_{28}H_{24}N_2O_4$ (MW: 452.51): C, 74.32; H, 5.35; N, 6.19; Found C, 74.30; H, 5.37; N, 6.20.

(3E,3′E)-3,3′-((1,10-phenanthroline-2,9-diyl)bis(methaneylylidene))bis(4,5,6-trimethoxyindolin-2-one) **8b**, Dark brown solid; Yield 27%; m.p.: 300–302 °C; IR (Nujol) ν_{max}: 1709 (s), 1620 (s), 1195 (m), 1135 (m), 1060 (m) cm^{-1}; ^1H NMR (DMSO–d_6): δ 3.74 (s, 6H, $2OCH_3$), 3.93 (s, 6H, $2OCH_3$), 4.07 (s, 6H, $2OCH_3$), 6.32 (s, 2H, ind-7), 8.01 (s, 2H, phen), 8.18 (s, 2H, 2CH), 8.46 (d, J = 8.4, 2H, phen), 8.85 (d, J = 8.4, 2H, phen), 10.60 (broad s, 2H, 2NH); MS (ES) *m/z*: 647.70 (M + H); Anal. Calcd for $C_{36}H_{30}N_4O_8$ (MW: 646.66): C, 66.87; H, 4.68; N, 8.66; Found C, 66.89; H, 4.67; N, 8.64.

(3E,3′E)-3,3′-((1,10-phenanthroline-2,9-diyl)bis(methaneylylidene))bis(5-methoxy-1-methylindolin-2-one) **8e,** Dark red solid; Yield 30%; m.p.: 296–298 °C; IR (Nujol) ν_{max}: 1703 (s), 1588 (m), 1281 (m), 1230 (m), 1020 (m) cm^{-1}; ^1H NMR (DMSO–d_6): δ 3.13 (s, 6H, $2OCH_3$), 3.28 (s, 6H, $2NCH_3$), 6.53 (dd, J = 8.4, 2.6, 2H, ind-6), 6.60 (d, J = 8.4, 2H, ind-7), 7.86 (s, 2H, phen), 8.08 (s, 2H, 2CH), 8.21 (d, J = 8.4, 2H, phen), 8.62 (d, J = 8.4, 2H, phen), 8.99 (d, J = 2.6, 2H, ind-4); MS (ES) *m/z*: 555.21 (M + H); Anal. Calcd for $C_{34}H_{26}N_4O_4$ (MW: 554.61): C, 73.63; H, 4.73; N, 10.10; Found C, 73.65; H, 4.70; N, 10.13.

(3E,3′E)-3,3′-((1,10-phenanthroline-2,9-diyl)bis(methaneylylidene))bis(1-benzylindolin-2-one) **8g**, Orange solid; Yield 27%; m.p.: 275–278 °C; IR (Nujol) ν_{max}: 1707 (s), 1608 (s), 1179 (m), 753 (m), 697 (m) cm^{-1}; ^1H NMR (DMSO–d_6): δ 4.99 (s, 4H, $2CH_2$), 6.70 (t, J = 7.7, 2H, ind), 6.74 (d, J = 7.7, 2H, ind), 6.97 (t, J = 7.7, 2H, ind), 7.31 (m, 10H, bz), 8.06 (s, 2H, phen), 8.15 (s, 2H, 2CH), 8.31 (d, J = 8.2, 2H, phen), 8.69 (d, J = 8.2, 2H, phen), 9.48 (d, J = 7.7, 2H, ind); MS (ES) *m/z*: 647.28 (M + H); Anal. Calcd for $C_{44}H_{30}N_4O_2$ (MW: 646.75): C, 81.71; H, 4.68; N, 8.66; Found C, 81.69; H, 4.70; N, 8.65.

(3E,3′E)-3,3′-((1,10-phenanthroline-2,9-diyl)bis(methaneylylidene))bis(1-(4-chlorobenzyl)indolin-2-one) **8i,** Dark yellow solid; Yield 25%; m.p.: 267–269 °C; IR (Nujol) ν_{max}: 1706 (s), 1603 (s), 1173 (m), 1091 (m), 1009 (m) cm^{-1}; ^1H NMR (DMSO–d_6): δ 4.99 (s, 4H, $2CH_2$), 6.69 (t, J = 7.6, 2H, ind), 6.74 (d, J = 7.6, 2H, ind), 6.99 (t, J = 7.6, 2H, ind), 7.34 (d, J = 8.4, 4H, ar), 7.40 (m, 4H, ar), 8.06 (s, 2H, phen), 8.14 (s, 2H, 2CH), 8.31 (d, J = 8.2, 2H, phen), 8.69 (d, J = 8.2, 2H, phen), 9.50 (d, J = 7.6, 2H, ind); MS (ES) *m/z*: 715.18 (M + H); Anal. Calcd for $C_{44}H_{28}Cl_2N_4O_2$ (MW: 715.63): C, 73.85; H, 3.94; N, 7.83; Found C, 73.83; H, 3.95; N, 7.84.

(3E,3′E)-3,3′-((1,10-phenanthroline-2,9-diyl)bis(methaneylylidene))bis(4,7-dimethoxyindolin-2-one) **8j,** Dark red solid; Yield 35%; m.p.: 302–305 °C; IR (Nujol) ν_{max}: 1690 (s), 1271 (s), 1158 (m), 1107 (m), 994 (m) cm^{-1}; ^1H NMR (DMSO–d_6): δ 3.75 (s, 6H, $2OCH_3$), 3.85 (s, 6H, $2OCH_3$), 6.65 (d, J = 8.8, 2H, ind), 6.95 (d, J = 8.8, 2H, ind), 8.00 (s, 2H, phen), 8.33 (s, 2H, 2CH), 8.43 (d, J = 8.4, 2H, phen), 8.79 (d, J = 8.4, 2H, phen), 10.80 (broad s, 2H, 2NH); MS (ES) *m/z*: 587.20 (M + H); Anal. Calcd for $C_{34}H_{26}N_4O_6$ (MW: 586.60): C, 69.62; H, 4.47; N, 9.55; Found C, 69.66; H, 4.44; N, 9.54.

(3E,3′E)-3,3′-((1,10-phenanthroline-2,9-diyl)bis(methaneylylidene))bis(5-chloroindolin-2-one) **8k**, Orange solid; Yield 37%; m.p.: 247–249 °C; IR (Nujol) ν_{max}: 3176 (w), 1716 (s), 1689 (m), 1614 (s), 1148 (m) cm^{-1}; ^1H NMR (DMSO–d_6): δ 6.56 (d, J = 8.2, 2H, ind-7), 6.96 (dd, J = 8.2, 2.0, 2H, ind-6), 7.86 (s, 2H, phen), 8.12 (s, 2H, 2CH), 8.25 (d, J = 8.4, 2H, phen), 8.66 (d, J = 8.4, 2H, phen), 9.61 (d, J = 2.0, 2H, ind-4), 10.57 (s, 2H, 2NH); MS (ES) *m/z*: 535.10 (M + H); Anal. Calcd for $C_{30}H_{16}Cl_2N_4O_2$ (MW: 535.38): C, 67.30; H, 3.01; N, 10.47; Found C, 67.32; H, 3.02; N, 10.44.

(3E,3′E)-3,3′-((1,10-phenanthroline-2,9-diyl)bis(methaneylylidene))bis(5-chloro-1-methylindolin-2-one) **8l**, Red solid; Yield 30%; m.p.: 287–289 °C; IR (Nujol) ν_{max}: 1714 (s), 1593 (s), 1265 (m), 1102 (s), 856 (s) cm^{-1}; ^1H NMR (DMSO–d_6): δ 3.19 (s, 6H, $2CH_3$), 6.73 (d, J = 8.4, 2H, ind-7), 7.04 (dd, J = 8.4, 2.2, 2H, ind-6), 7.96 (s, 2H, phen), 8.14 (s, 2H, 2CH), 8.28 (d, J = 8.4, 2H, phen), 8.68 (d, J = 8.4, 2H, phen), 9.57 (d, J = 2.2, 2H, ind-4); MS (ES) *m/z*: 563.14 (M + H); Anal. Calcd for $C_{32}H_{20}Cl_2N_4O_2$ (MW: 563.44): C, 68.22; H, 3.58; N, 9.94; Found C, 68.24; H, 3.55; N, 9.95.

(3E,3′E)-3,3′-((1,10-phenanthroline-2,9-diyl)bis(methaneylylidene))bis(5-methoxy-6-methylindolin-2-one) **8m**, Black solid; Yield 40%; m.p.: 284–287 °C; IR (Nujol) ν_{max}: 1697 (s), 1619 (s), 1189 (m), 1107 (m), 1025 (m) cm^{-1}; ^1H NMR (DMSO–d_6): δ 1.95 (s, 6H, $2CH_3$), 3.25 (s, 6H, $2OCH_3$), 6.27 (s, 2H, ind), 7.63 (s, 2H, phen), 8.07 (s, 2H, 2CH), 8.17 (d, J = 8.2, 2H, phen), 8.56 (s, 2H, ind), 8.61 (d, J = 8.2, 2H, phen), 10.12 (s, 2H, 2NH); MS (ES) *m/z*: 555.29 (M + H); Anal. Calcd for $C_{34}H_{26}N_4O_4$ (MW: 554.61): C, 73.63; H, 4.73; N, 10.10; Found C, 73.60; H, 4.75; N, 10.12.

(3E,5E)-3,5-bis((2-chloro-5-(dimethylamino)-1H-indol-3-yl)methylene)-1,7-dimethyl-5,7-dihydropyrrolo [3,2-f]indole-2,6(1H,3H)-dione **11n**, Red solid; Yield 20%; m.p.: 298–301 °C; IR (Nujol) ν_{max}: 3220 (m), 1690 (s), 1615 (s), 1274 (m), 1125 (m) cm^{-1}; ^1H NMR (DMSO–d_6): δ 2.42 (s, 12H, s, 2 $N(CH_3)_2$), 3.31 (s, 6H, $2CH_3$), 5.64 (d, J = 2.5, 2H, ind-4), 6.37 (dd, J = 8.8, 2.5, 2H, ind-6), 6.57 (s, 1H, ar), 6.90 (m, 3H, 2ind-7 + ar), 7.48 (s, 2H, 2CH), 12.04 (s, 2H, 2NH); MS (ES) *m/z*: 625.21 (M + H); Anal. Calcd for $C_{34}H_{30}Cl_2N_6O_2$ (MW: 625.55): C, 65.28; H, 4.83; N, 13.43; Found C, 65.27; H, 4.84; N, 13.42.

(3E,5E)-3,5-bis((2-chloro-5-methoxy-1H-indol-3-yl)methylene)-1,7-dimethyl-5,7-dihydropyrrolo [3,2-f]indole-2,6(1H,3H)-dione **11o**, Black solid; Yield 30%; m.p.: 288–300 °C; IR (Nujol) ν_{max}: 3175 (m), 1682 (s), 1607 (s), 1276 (m), 1122 (m) cm^{-1}; ^1H NMR (DMSO–d_6): δ 3.22 (s, 6H, $2OCH_3$), 3.33 (s, 6H, $2NCH_3$), 5.89 (d, J = 2.5, 2H, ind-4), 6.46 (dd, J = 8.8, 2.5, 2H, ind-6), 6.60 (s, 1H, ar), 6.93 (s, 1H, ar), 6.97 (d, J = 8.8, 2H, ind-7), 7.46 (s, 2H, 2CH), 12.18 (s, 2H, 2NH); MS (ES) *m/z*: 599.30 (M + H); Anal. Calcd for $C_{32}H_{24}Cl_2N_4O_4$ (MW: 599.47): C, 64.12; H, 4.04; N, 9.35; Found C, 64.15; H, 4.02; N, 9.36.

(3E,5E)-3,5-bis((5-methoxy-1H-indol-3-yl)methylene)-1,7-dimethyl-5,7-dihydropyrrolo [3,2-f]indole-2,6(1H,3H)-dione **11p**, Red solid; Yield 78%; m.p.: 300 °C, dec; IR (Nujol) ν_{max}: 3257 (s), 1670 (s), 1624 (s), 1219 (s), 1081 (s) cm^{-1}; ^1H NMR (DMSO–d_6): δ 3.34 (s, 6H, $2OCH_3$), 3.93 (s, 6H, $2NCH_3$), 6.82 (s, 1H, ar), 6.88 (d, J = 8.8, 2H, ind-6), 7.42 (d, J = 8.8, 2H, ind-7), 7.75 (s, 2H, ind-4), 8.16 (s, 2H, 2CH), 8.51 (s, 1H, ar), 9.32 (s, 2H, ind-2), 11.93 (s, 2H, 2NH); MS (ES) *m/z*: 531.24 (M + H); Anal. Calcd for $C_{32}H_{26}N_4O_4$ (MW: 530.58): C, 72.44; H, 4.94; N, 10.56; Found C, 72.43; H, 4.95; N, 10.54.

(3E,5E)-3,5-bis((1-benzyl-2-chloro-1H-indol-3-yl)methylene)-1,7-

dimethyl-5,7-dihydropyrrolo [3,2-f]indole-2,6(1H,3H)-dione **11q**, Red solid; Yield 44%; m.p.: 268–281 °C; IR (Nujol) ν_{max}: 1701 (s), 1606 (s), 1271 (m), 1127 (m), 825 (m) cm^{-1}; ^1H NMR (DMSO–d_6): δ 5.56 (s, 4H, $2CH_2$), 6.44 (s, 1H, ar), 6.56 (d, $J = 7.7$, 2H, ind), 6.68 (t, $J = 7.7$, 2H, ind), 6.94 (s, 1H, ar), 7.03 (t, $J = 7.7$, 2H, ind), 7.17 (d, $J = 7.8$, 4H, bz), 7.31 (m, 6H, bz), 7.40 (s, 2H, 2CH), 7.57 (d, $J = 7.7$, 2H, ind); MS (ES) *m/z*: 719.22 (M + H); Anal. Calcd for $C_{44}H_{32}Cl_2N_4O_2$ (MW: 719.67): C, 73.43; H, 4.48; N, 7.79; Found C, 73.44; H, 4.47; N, 7.81.

(3E,5E)-3,5-bis((1-benzyl-2-chloro-5-methoxy-6-methyl-1H-indol-3-yl) methylene)-1,7-dimethyl-5,7-dihydropyrrolo [3,2-f]indole-2,6(1H,3H)-dione **11r**, Brownish solid; Yield 75%; m.p.: 250 °C, dec; IR (Nujol) ν_{max}: 1711 (s), 1620 (s), 1274 (m), 1123 (m), 1044 (m) cm^{-1}; ^1H NMR (DMSO–d_6): δ 2.18 (s, 6H, $2CH_3$), 3.22 (s, 6H, $2OCH_3$), 3.33 (s, 6H, $2NCH_3$), 5.49 (s, 4H, $2CH_2$), 5.97 (s, 2H, ind), 6.69 (s, 1H, ar), 6.94 (s, 1H, ar, 7.09 (m, 4H, 2ind + 2bz), 7.30 (m, 8H, bz), 7.46 (s, 2H, 2CH); MS (ES) *m/z*: 807.27 (M + H); Anal. Calcd for $C_{48}H_{40}Cl_2N_4O_4$ (MW: 807.77): C, 71.37; H, 4.99; N, 6.94; Found C, 71.38; H, 4.98; N, 6.96.

(3E,5E)-3,5-bis((2-chloro-1-methyl-1H-indol-3-yl)methylene)-1,7-dimethyl-5,7-dihydropyrrolo [3,2-f]indole-2,6(1H,3H)-dione **11s**, Brown solid; Yield 32%; m.p.: 300 °C, dec; IR (Nujol) ν_{max}: 1696 (s), 1624 (s), 1270 (s), 1176 (s), 1106 (s) cm^{-1}; ^1H NMR (DMSO–d_6): δ 3.30 (s, 6H, $2NCH_3$), 3.74 (s, 6H, $2NCH_3$), 6.44 (s, 1H, ar), 6.50 (d, $J = 7.4$, 2H, ind), 6.63 (t, $J = 7.4$, 2H, ind), 6.95 (m, 3H, ar + 2ind), 7.40 (m, 4H, 2CH + 2ind); MS (ES) *m/z*: 567.14 (M + H); Anal. Calcd for $C_{32}H_{24}Cl_2N_4O_2$ (MW: 567.47): C, 67.73; H, 4.26; N, 9.87; Found C, 67.76; H, 4.24; N, 9.86.

(3E,5E)-3,5-bis((2-chloro-1-phenyl-1H-indol-3-yl)methylene)-1,7-dimethyl-5,7-dihydropyrrolo [3,2-f]indole-2,6(1H,3H)-dione **11t**, Red solid; Yield 55%; m.p.: 282–284 °C; IR (Nujol) ν_{max}: 1704 (s), 1614 (s), 1270 (m), 1117 (m), 740 (m) cm^{-1}; ^1H NMR (DMSO–d_6): δ 3.34 (s, 6H, $2NCH_3$), 6.91 (m, 12H, 6ind + 2ar + 4bz), 7.12 (m, 2H, ind), 7.44 (m, 6H, bz), 7.58 (s, 2H, 2CH); MS (ES) *m/z*: 691.16 (M + H); Anal. Calcd for $C_{42}H_{28}Cl_2N_4O_2$ (MW: 691.61): C, 72.94; H, 4.08; N, 8.10; Found C, 72.92; H, 4.09; N, 8.12.

(3E,5E)-3,5-bis((2-chloro-5-hydroxy-6-methyl-1H-indol-3-yl)methylene)-1,7-dimethyl-5,7-dihydropyrrolo [3,2-f]indole-2,6(1H,3H)-dione **11u**, Dark red solid; Yield 25%; m.p.: 289–292 °C; IR (Nujol) ν_{max}: 3200 (s), 1674 (s), 1602 (s), 1265 (m), 1107 (m) cm^{-1}; ^1H NMR (DMSO–d_6): δ 2.14 (s, 6H, $2CH_3$), 3.31 (s, 6H, $2NCH_3$), 5.81 (s, 2H, ind), 6.53 (s, 1H, ar), 6.81 (s, 2H, ind), 6.86 (s, 1H, ar), 7.37 (s, 2H, 2CH), 8.29 (s, 2H, 2OH) 11.67 (s, 2H, 2NH); MS (ES) *m/z*: 599.14 (M + H); Anal. Calcd for $C_{32}H_{24}Cl_2N_4O_4$ (MW: 599.47): C, 64.12; H, 4.04; N, 9.35; Found C, 64.13; H, 4.05; N, 9.33.

(3E,5E)-3,5-bis((2-chloro-5-methoxy-6-methyl-1H-indol-3-yl)methylene)-1,7-dimethyl-5,7-dihydropyrrolo [3,2-f]indole-2,6(1H,3H)-dione **11v**, Brown solid; Yield 55%; m.p.: 298–300 °C; IR (Nujol) ν_{max}: 3216 (m), 1675 (m), 1603 (s), 1270 (m), 1122 (m) cm^{-1}; ^1H NMR (DMSO–d_6): δ 2.16 (s, 6H, $2CH_3$), 3.15 (s, 6H, $2OCH_3$), 3.33 (s, 6H, $2NCH_3$), 5.82 (s, 2H, ind), 6.73 (s, 1H, ar), 6.83 (s, 2H, ind), 6.92 (s, 1H, ar), 7.46 (s, 2H, 2CH), 12.03 (s, 2H, 2NH); MS (ES) *m/z*: 627.15 (M + H); Anal. Calcd for $C_{34}H_{28}Cl_2N_4O_4$ (MW: 627.52): C, 65.08; H, 4.50; N, 8.93; Found C, 65.06; H, 4.52; N, 8.94.

(3E,5E)-3,5-bis((2-chloro-1-(4-chlorobenzyl)-5-methoxy-1H-indol-3-yl)methylene)-1,7-dimethyl-5,7-dihydropyrrolo [3,2-f]indole-2,6(1H,3H)-dione **11w**, Brown solid; Yield 43%; m.p.: 300 °C, dec; IR (Nujol) ν_{max}: 1708 (s), 1613 (s), 1271 (m), 1194 (m), 1120 (m) cm^{-1}; ^1H NMR (DMSO–d_6): δ 3.25 (s, 6H, $2OCH_3$), 3.33 (s, 6H, $2NCH_3$), 5.54 (s, 4H, $2CH_2$), 5.98 (s, 2H, ind), 6.60 (m, 3H, ar + 2ind), 6.96 (s, 1H, ar), 7.19 (m, 4H, bz), 7.42 (m, 8H, 4bz + 2ind + 2CH); MS (ES) *m/z*: 847.14 (M + H); Anal. Calcd for $C_{46}H_{34}Cl_4N_4O_4$ (MW: 848.60): C, 65.11; H, 4.04; N, 6.60; Found C, 65.13; H, 4.02; N, 6.61.

(3E,5E)-3,5-bis((2-chloro-1-(4-chlorobenzyl)-5-methoxy-6-methyl-1H-indol-3-yl)methylene)-1,7-dimethyl-5,7-dihydropyrrolo [3,2-f]indole-2,6 (1H,3H)-dione **11x**, Brownish solid; Yield 50%; m.p.: 280 °C, dec; IR (Nujol) ν_{max}: 1697 (s), 1608 (s), 1272 (s), 1109 (m), 845 (m) cm^{-1}; ^1H NMR (DMSO–d_6): δ 2.17 (s, 6H, $2CH_3$), 3.22 (s, 6H, $2OCH_3$), 3.31 (s, 6H, $2NCH_3$), 5.48 (s, 4H, $2CH_2$), 5.97 (s, 2H, ind), 6.68 (s, 1H, ar), 6.94 (s, 1H, ar), 7.09 (d, $J = 8.4$, 4H, bz), 7.22 (s, 2H, ind), 7.38 (d, $J = 8.4$, 4H, bz), 7.45 (s, 2H, 2CH); MS (ES) *m/z*: 875.20 (M + H); Anal. Calcd for $C_{48}H_{38}Cl_4N_4O_4$ (MW: 876.66): C, 65.76; H, 4.37; N, 6.39; Found C, 65.78; H, 4.36; N, 6.40.

*4.1.1.2. Method 2 (compound **5c**).* The oxindole **1c** (10 mmol) was dissolved in ethanol (100 mL) and treated with the aldehyde **2** (5 mmol) and 37% hydrochloric acid (1 mL). The reaction mixture was refluxed for 6 h (according to a TLC test) and cooled. The yellow to orange precipitate thus formed was collected by filtration. The crude product was purified by crystallization with ethanol.

(3E,3′Z)-3,3′-((5-(tert-butyl)-2-hydroxy-1,3-phenylene)bis(methaneylylidene))bis(4,7-dichloroindolin-2-one) **5c,** Orange solid; Yield 23%; m.p.: 305 °C, dec; IR (Nujol) ν_{max}: 3449 (m), 3176 (m), 1712 (s), 1164 (s), 929 (m) cm^{-1}; ^1H NMR (DMSO–d_6): δ 1.43 (s, 9H, $3CH_3$), 7.17 (d, $J =$ 8.8, 1H, ind), 7.39 (d, $J = 8.8$, 1H, ind), 7.42 (d, $J = 8.8$, 1H, ind), 7.63 (d, $J = 8.8$, 1H, ind), 8.37 (d, $J = 2.6$, 1H, ar), 8.63 (d, $J = 2.6$, 1H, ar), 8.78 (s, 1H, CH), 9.23 (s, 1H, CH), 11.30 (s, 2H, 2NH); MS (ES) *m/z*: 573.05 (M + H); Anal. Calcd for $C_{28}H_{20}Cl_4N_2O_3$ (MW: 574.28): C, 58.56; H, 3.51; N, 4.88; Found C, 58.53; H, 3.54; N, 4.87.

*4.1.1.3. Method 3 (compounds **7a, d, f, j**).* The appropriate oxindole **1** (10 mmol) was dissolved in acetic acid (50 mL) and treated with isophthaldehyde **3** (5 mmol) and 37% hydrochloric acid (1 mL). The reaction mixture was refluxed for 4 h and the solid separated on cooling was collected by filtration. The crude products were purified by crystallization with ethanol. **7j** was purified by column chromatography.

(3E,3′E)-3,3′-(1,3-phenylenebis(methaneylylidene))bis(4-fluoroindolin-2-one) **7a**, Yellow solid; Yield 24%; m.p.: 238–240 °C; IR (Nujol) ν_{max}: 3514–3150 (m), 1708 (s), 1619 (s), 1150 (m) cm^{-1}; ^1H NMR (DMSO–d_6): δ 6.68 (m, 4H, 2ind + 2ar), 7.48 (dd, $J = 8.4$, 5.6, 2H, ind), 7.65 (s, 2H, 2CH), 7.68 (m, 1H, ar), 7.80 (d, $J = 8.4$, 2H, ind), 7.90 (m, 1H, ar), 10.81 (s, 2H, 2NH); MS (ES) *m/z*: 401.13 (M + H); Anal. Calcd for $C_{24}H_{14}F_2N_2O_2$ (MW: 400.38): C, 72.00; H, 3.52; N, 7.00; Found C, 72.02; H, 3.50; N, 7.01.

(3E,3′E)-3,3′-(1,3-phenylenebis(methaneylylidene))bis(5-fluoroindolin-2-one) **7d**, Orange solid; Yield 75%; m.p.: 317–318 °C; IR (Nujol) ν_{max}: 3457 (m), 3172 (m), 1709 (s), 1621 (s), 1187 (m) cm^{-1}; ^1H NMR (DMSO–d_6): δ 6.87(dd, $J = 8.0$, 4.8, 2H, ind), 7.11 (m, 4H, ind), 7.73 (t, $J = 8.0$, 1H, ar), 7.76 (s, 2H, 2CH), 7.83 (d, $J = 8.0$, 2H, ar), 7.92 (s, 1H, ar), 10.67 (s, 2H, 2NH); MS (ES) *m/z*: 401.12 (M + H); Anal. Calcd for $C_{24}H_{14}F_2N_2O_2$ (MW: 400.38): C, 72.00; H, 3.52; 7.00; Found C, 72.01; H, 3.53; 7.00.

(3E,3′E)-3,3′-(1,3-phenylenebis(methaneylylidene))bis(6-chloroindolin-2-one) **7f**, Yellow solid; Yield 68%; m.p.: 282–284 °C; IR (Nujol) ν_{max}: 3662–3100 (m), 1714 (s), 1608 (s), 1071 (m) cm^{-1}; ^1H NMR (DMSO–d_6): δ 6.91 (m, 4H, ind), 7.46 (d, $J = 8.8$, 2H, ind-4), 7.68 (m, 1H, ar), 7.71 (s, 2H, 2CH), 7.82 (d, $J = 7.4$, 2H, ar), 7.92 (s, 1H, ar), 10.82 (s, 2H, 2NH); MS (ES) *m/z*: 433.05 (M + H); Anal. Calcd for $C_{24}H_{14}Cl_2N_2O_2$ (MW: 433.29): C, 66.53; H, 3.26; N, 6.47; Found C, 66.54; H, 3.24; N, 6.48.

(3E,3′E)-3,3′-(1,3-phenylenebis(methaneylylidene))bis(4,7-dimethoxyindolin-2-one) **7j**, Red solid; Yield 13%; m.p.: 244–246 °C; IR (Nujol) ν_{max}: 3155 (s), 1685 (s), 1602 (s), 1254 (s), 1117 (s) cm^{-1}; ^1H NMR (DMSO–d_6): δ 3.78 (s, 6H, $2OCH_3$), 3.91 (s, 6H, $2OCH_3$), 6.62 (d, $J = 9.0$, 2H, ind), 6.91 (d, $J = 9.0$, 2H, ind), 7.46 (t, $J = 8.0$, 1H, ar), 8.10 (s, 2H, 2CH), 8.30 (d, $J = 8.0$, 2H, ar), 8.57 (s, 1H, ar), 10.64 (s, 2H, 2NH); MS (ES) *m/z*: 485.17 (M + H); Anal. Calcd for $C_{28}H_{24}N_2O_6$ (MW: 484.51): C, 69.41; H, 4.99; N, 5.78; Found C, 69.39; H, 5.00; N, 5.77.

*4.1.1.4. Method 4 (compound **7g**).* Isophthaldehyde **3** (5 mmol) was dissolved in toluene (75 mL) and treated with 1-benzylindolin-2-one **1g** (15 mmol) in the presence of 4-toluenesulfonic acid (0.5 mmol). The reaction mixture was maintained under stirring at room temperature for

80 h, the precipitate formed was collected by filtration. The crude derivative was purified by column chromatography.

(3E,3′E)-3,3′-(1,3-phenylenebis(methaneylylidene))bis(1-benzylindolin-2-one) **7g**, Yellow solid; Yield 44%; m.p.: 295–296 °C; IR (Nujol) ν_{max}: 1706 (s), 1606 (m), 1169 (m), 1103 (w) cm^{-1}; ^1H NMR (DMSO–d_6): δ 4.99 (s, 4H, $2CH_2$), 6.89 (t, $J = 7.6$, 2H, ind), 6.99 (d, $J = 7.6$, 2H, ind), 7.26 (m, 5H, 2ind + 2bz + ar), 7.34 (m, 8H, bz), 7.53 (d, $J = 7.6$, 2H, ind), 7.68 (t, $J = 7.8$, 1H, ar), 7.87 (m, 3H, 2CH + ar), 8.00 (s, 1H, ar); MS (ES) *m/z*: 545.23 (M + H); Anal. Calcd for $C_{38}H_{28}N_2O_2$ (MW: 544.65): C, 83.80; H, 5.18; N, 5.14; Found C, 83.78; H, 5.18; N, 5.16.

4.2. Biology

4.2.1. NCI screening

To test the cytostatic and cytotoxic impact of the synthetic compounds, the NCI-60 Human Tumor Cell Lines Screening has been used. Leukemia, Melanoma, NSCLC, Colon, CNS, Ovarian, Renal, and Breast cancer cells (https://dtp.cancer.gov/discovery_development/nci-60/cell_list.htm) were seeded in a 96 multi-well plate at a cell density of 5 $\times 10^3$ - 4 $\times 10^4$ cells/well, depending on the cell line, as described [44]. Compounds subjected to the full 5-concentration assay (**5a**, **5b**, **5d**, **5e**, **5f**, **6**, **7a**, **7d**, **7f**, **7j**, **8b**, **8e**, **8k**, **8m**, **11n**, **11o**, **11v**) and vincristine sulfate were diluted in fresh media and added to the cells at scalar concentration 0–1000 μM or 0–100 μM. Briefly, endpoint determinations of the cell viability or cell growth were performed at 48 h of treatment by in situ fixation of cells, which was followed by staining with a protein-binding dye, sulforhodamine B (SRB) (https://dtp.cancer.gov/discovery_development/nci-60/methodology.htm).

After washing, SRB optical density was measured spectrophotometrically. TGI, LC_{50}, and GI_{50} were established according to the NCI screening procedures (https://dtp.cancer.gov/discovery_development/nci-60/methodology.htm).

4.2.2. Cell culture and treatments

HDFa human dermal fibroblast as control cell line were purchased from American Type Culture Collection (ATCC, Manassas, VA). The human ovarian cancer cell line IGROV1 has been kindly provided by Prof. Colnaghi (Istituto Nazionale Tumori; IRCCS) (Milan, Italy). Cells were cultured in RPMI 1640 medium (Euroclone, Milan, Italy), supplemented with 10% FCS (Euroclone, Milan, Italy) and 2 mM l-glutamine (Sigma-Aldrich, Milan, Italy), at 37 °C, and a 5% CO_2 atmosphere. Compound **5f** was dissolved in DMSO in a 30 mM stock solution. In cell treatments, the final DMSO concentration never exceeded 0.1%.

4.2.3. MTT assay

IGROV1 and HDFa cells were seeded at 1.5 $\times 10^4$ cells/well in a 96-well culture plastic plate (Sarstedt, Milan, Italy), and after 24 h of growth they were exposed to increasing concentrations of **5f** (from 0.010 μM to 500 μM) solubilized in RPMI 1640 medium. After 24 h of treatment, the culture medium was replaced with 100 μL of 3-(4,5-dimethylthiazolyl-2)-2,5-diphenyltetrazolium bromide (MTT) (Sigma-Aldrich, Milan, Italy) dissolved in Phosphate Buffer Solution (PBS) at the concentration of 0.2 mg/mL, and samples were incubated for 2 h at 37 °C. The absorbance at 570 nm was measured using a multiwell plate reader (Tecan, Männedorf, CH), and data were analyzed by Prism GraphPad software, and expressed as IC_{50} μM.

4.2.4. Quantitative phase image (QPI) microscopy

Quantitative phase image (QPI) microscopy assay was performed using the Livecyte microscope (Phase Focus Limited, Sheffield, UK) according to manufacturer's indications. In brief, IGROV1 and HDFa were seeded in a 96-well plate (Sarstedt, Milan, Italy) at 4 $\times 10^3$ per well. After 24 h cells were treated with **5f** 5 μM in six replicates and the images were acquired every 60 min for 2 days using a 10× objective (0.25 NA), at 37 °C and 5% CO_2. Data were analyzed using the Cell Analysis Toolbox software version 3.10.0 (Phase Focus Limited, Sheffield, UK) to evaluate cell growth, doubling times, and motility.

4.2.5. Cell cycle analysis

IGROV1 were plated at density of 2 $\times 10^4$ cell/cm^2 in a Petri dish and after 24 h treated with 5 μM **5f** for 24 h. Untreated and treated cells were detached, washed in PBS and the pellet was finally re-suspended in 0.01% Igepal (Sigma-Aldrich, Milan, Italy), 10 μg/mL RNase (Sigma-Aldrich, Milan, Italy), 0.1% sodium citrate (Sigma-Aldrich, Milan, Italy), 50 μg/mL propidium iodide (PI) (Sigma-Aldrich, Milan, Italy), for 30 min at room temperature in the dark. Flow cytometric assays were performed on a Cell Sorter Bio-Rad S3e (Bio-Rad, Watford, UK).

4.2.6. Histone post-translational modification

IGROV1 were seeded at density of 1,5 $\times 10^4$ cell/cm^2 in a Petri dish and after 48 h treated for 6 h with compound **5f** at a final concentration of 5 μM. For the DNA damage assay, cells were cultured as above and treated with **5f** for 24 h and then they were irradiated with an UV lamp 7,5 Watt for 3 min. As a positive control cells were treated with UV radiation, that induces global DNA damage. Cells were harvested, washed with 10 mM sodium butyrate in PBS, and nuclei were isolated according to Micheletti [45]. In brief, the nuclear pellet was resuspended in 0.2 mL of 0.4 N H_2SO_4 solution. The suspension was centrifuged, and the supernatant was taken and mixed with 1 mL of acetone. The histone pellets were collected by microcentrifugation and air-dried at room temperature. The histone fractions were solubilized in 20 μL of H_2O. Histone proteins were quantified using a protein assay kit (Bio--Rad, Hercules, CA, USA). Successively, histone modifications were detected using Western Blotting. The samples were resolved on a 15% gel in Tris/Glycine buffer at 150 V for 90 min. The nitrocellulose membrane was incubated overnight at 4 °C with mouse anti-acetylated lysines (Millipore, Billerica, MA, USA) or rabbit anti-γH2Ax (Santa Cruz, CA, USA) primary antibodies. After washes with PBS-polyoxyethylene sorbitan monolaurate 0.1% (TWEEN 20) (St. Louis, MO, US), the membrane was incubated with mouse or rabbit secondary horseradish peroxidase-conjugated antibody (GE Healthcare, Chicago, Il, US). Antibody binding was detected by Amersham ECL Plus Western Blotting Detection System (GE Healthcare, Chicago, Il, US). SDS-PAGE (sodium dodecyl sulfate-polyacrylamide gel electrophoresis) was stained with Coomassie Brilliant Blue R-250 (Bio-Rad, Hercules, CA, USA). Densitometric analyses were performed using a Fluor-S Max MultiImager (Bio-Rad, Hercules, CA, USA), and relative quantification of histone acetylation and histone H2Ax phosphorylation signals was performed using densitometry and normalized to the H1 signal as a control.

4.2.7. Western blot and protein analysis

IGROV1 cells were seeded and treated as described above. Cells were then washed with PBS and incubated with the lysis buffer radio immunoprecipitation assay (RIPA) at 4 °C for 15 min with agitation. After cell lysis, the solution was centrifuged for 20 min at full speed and the supernatant containing the proteins was quantified using the Bio-Rad protein assay (Bio-Rad, Hercules, CA, US). Proteins were analyzed by sodium dodecyl sulfate-polyacrylamide gel electrophoresis (SDS-PAGE) and Western blot on a nitrocellulose membrane. Samples were resolved on a 12.5% or 7.5% density gel in Tris/Glycine buffer at 150 V for 90 min. After electrophoresis and Western blot, the nitrocellulose membrane was initially blocked by incubation with PBS-TWEEN 20 0.1% in agitation for 1 h, then it was incubated overnight at 4 °C with anti-cyclin D1, or anti-RAD51, or anti-α5 subunit of α5β1 integrin, or α-tubulin primary antibodies (Santa Cruz, CA, USA) diluted in PBS-TWEEN 20 0.1%. After washes with PBS-TWEEN 20 0.1%, the membrane was incubated for 1 h with secondary horseradish peroxidase-conjugated antibody (GE Healthcare, Chicago, Il, US), and then antibody binding was detected by Bio-Rad and quantification was done by a Fluor-S Max MultiImager (Bio-Rad, Hercules, CA, US) using α-tubulin signal as control.

4.2.8. siRNA silencing

siRNA silencing was applied on IGROV1 cells after 72 h of adhesion, when cells were 70–80% confluent. The specific siRNA against CCND1 gene expression and the scramble siRNA were transfected using lipofectamine according to the manufacturer's specifications (Thermo Fisher Scientific, Waltham, MS, US). Control siRNA or CCND1 siRNA (10 nM) were used to treat cells in phenol red-, serum, and antibiotic-free RPMI. After 24 h of siRNA treatment, the medium was changed in complete RPMI 1640 medium, and cells were analyzed 24 h after medium change.

4.2.9. RNA extraction, reverse transcription and qRT-PCR

For the RNA extraction, the RNeasy Mini Kit (Qiagen, Hilden, Germany) was used. Pelleted cells were lysed with 350 μL of RLT lysis buffer prepared by adding 10 μL of β-mercaptoethanol (Sigma-Aldrich, Milan, Italy) to 1 mL of buffer, according to the manufacturer's protocol. RNA extracted was eluted by adding 30 μL of RNase-free water directly on the membrane of the column. The membrane was hydrated for 3 min at room temperature and then centrifuged at 8000 *g* for 1 min. RNA was quantified by NanoDrop spectrophotometer (Thermo Fisher Scientific, Waltham, MS, US). RNA was employed to generate cDNA using the Transcriptor High Fidelity cDNA Synthesis Kit (Euroclone, Milan, Italy). cDNA was used to analyze the levels of transcripts by quantitative Real-Time PCR (qRT-PCR). The Takara kit (Takara Bio, Kusatsu, Japan) and the LightCycler 2.0 Instrument (Roche Diagnostic, Basel, Switzerland) were employed. The first gene analyzed was the house-keeping gene β-actin and its C_T values were used as standards in the $\Delta\Delta C_T$ method of results analysis. cDNA samples from IGROV1 treated/irradiated cells were compared to vehicle. As blank control, a reaction mixture without the sample was always used. Samples were analyzed at least in triplicate and Student's t-test was used to verify the significance of results (a p-value less than 0.05 was considered significant). Primers (Sigma-Aldrich, Milan, Italy) employed are reported in S.I. (Table S1).

5. Statistical analysis

All experiments were performed at least in triplicates on three independent samples. The data were processed using one-way analysis of variance (ANOVA) followed by Dunnett's multiple comparison test. Group differences were considered significant when $p \leq 0.05$. Statistical analysis was carried out by GraphPad Prism Software (version 5.0c, GraphPad Software, San Diego, CA, USA).

Disclaimer

The content of this paper is solely the responsibility of the authors and does not necessarily reflect the official views of the National Institutes of Health.

CRediT authorship contribution statement

Rita Morigi: Writing – review & editing, Writing – original draft, Supervision, Investigation, Data curation, Conceptualization. **Chiara Zalambani:** Writing – review & editing, Methodology, Formal analysis. **Giovanna Farruggia:** Supervision, Data curation, Conceptualization, Writing – original draft, Writing – review & editing. **Laura Verardi:** Formal analysis. **Daniele Esposito:** Investigation, Methodology, Writing – review & editing. **Alberto Leoni:** Investigation, Methodology, Writing – review & editing. **Francesca Borsetti:** Formal analysis. **Manuela Voltattorni:** Formal analysis. **Laura Zambonin:** Formal analysis. **Luca Pincigher:** Formal analysis, Methodology. **Natalia Calonghi:** Writing – review & editing, Writing – original draft, Conceptualization, Data curation, Supervision. **Alessandra Locatelli:** Writing – review & editing, Writing – original draft, Supervision, Investigation, Data curation, Conceptualization.

Declaration of competing interest

The authors declare that they have no known competing financial interests or personal relationships that could have appeared to influence the work reported in this paper.

Data availability

Data will be made available on request.

Acknowledgement

We are grateful to Lanfranco Masotti for the helpful discussions. We also wish to acknowledge Tullia Maraldi (University of Modena and Reggio Emilia, Modena, Italy) for the license to use BioRender.com to create the graphical abstract. We are grateful to the Center for Applied Biomedical Research – CRBA (University of Bologna) for the use of Lifecyte Microscopy and National Cancer Institute (Bethesda, MD) for the anticancer tests. This work was supported in part by a grant from the University of Bologna, Italy (RFO).

Appendix A. Supplementary data

Supplementary data to this article can be found online at https://doi.org/10.1016/j.ejmech.2024.116365.

Abbreviations

CA-4, combretastatin A-4; CA-4P, combretastatin 4-A phosphate; PI, propidium iodide; PS, phosphatidylserine; PARP, polyADP-ribose polymerase; PBL, peripheral blood lymphocytes; PHA, phytohemaglutinin; FITC, fluorescein isothiocyanate; BSA, bovine serum albumin; PBS, phosphate-buffered saline; SDS-PAGE, sodium dodecyl sulfate polyacrylamide gel electrophoresis.

References

[1] B.B.E. Barnes, K. Steindorf, R. Hein, D. Flesch-Janys, J. Chang-Claude, Population attributable risk of invasive postmenopausal breast cancer and breast cancer subtypes for modifiable and non-modifiable risk factors, Cancer Epidemiol 35 (2011) 345–352, https://doi.org/10.1016/j.canep.2010.11.003.

[2] W.S. Dalton, Mechanisms of drug resistance in hematologic malignancies, Semin. Hematol. 34 (1997) 3–8.

[3] A.M. Young, C.E. Allen, K.L. Audus, Efflux transporters of the human placenta, Adv. Drug Deliv. Rev. 55 (2003) 125–132, https://doi.org/10.1016/S0169-409X(02)00174-6.

[4] S.B. Coburn, F. Bray, M.E. Sherman, B. Trabert, International patterns and trends in ovarian cancer incidence, overall and by histologic subtype: ovarian cancer trends, Int. J. Cancer 140 (2017) 2451–2460, https://doi.org/10.1002/ijc.30676.

[5] M. Seoud, E.Å. Lundqvist, K. Fujiwara, Targeted therapy in gynecologic cancers: ready for prime time? Int. J. Gynecol. Obstet. 131 (2015) S150–S152, https://doi.org/10.1016/j.ijgo.2015.06.012.

[6] A. Leoni, A. Locatelli, R. Morigi, M. Rambaldi, 2-Indolinone a versatile scaffold for treatment of cancer: a patent review (2008–2014), Expert Opin. Ther. Pat. 26 (2016) 149–173, https://doi.org/10.1517/13543776.2016.1118059.

[7] A. Andreani, S. Bellini, S. Burnelli, M. Granaiola, A. Leoni, A. Locatelli, R. Morigi, M. Rambaldi, L. Varoli, N. Calonghi, et al., Substituted *E* -3-(3-Indolylmethylene)-1,3-Dihydroindol-2-Ones with antitumor activity. In depth study of the effect on growth of breast cancer cells, J. Med. Chem. 53 (2010) 5567–5575, https://doi.org/10.1021/jm1007165.

[8] A. Andreani, M. Granaiola, A. Locatelli, R. Morigi, M. Rambaldi, L. Varoli, N. Calonghi, C. Cappadone, G. Farruggia, C. Stefanelli, et al., Substituted 3-(5-imidazo[2,1- *b*]Thiazolylmethylene)-2-Indolinones and analogues: synthesis, cytotoxic activity, and study of the mechanism of action, J. Med. Chem. 55 (2012) 2078–2088, https://doi.org/10.1021/jm2012694.

[9] A. Leoni, A. Locatelli, R. Morigi, M. Rambaldi, C. Cappadone, G. Farruggia, S. Iotti, L. Merolle, M. Zini, C. Stefanelli, Substituted E-3-(3-indolylmethylene)1,3-dihydroindol-2-ones with antiproliferative activity. Study of the effects on HL-60 leukemia cells, Eur. J. Med. Chem. 79 (2014) 382–390, https://doi.org/10.1016/j.ejmech.2014.04.004.

[10] R. Morigi, A. Locatelli, A. Leoni, M. Rambaldi, R. Bortolozzi, E. Mattiuzzo, R. Ronca, F. Maccarinelli, E. Hamel, R. Bai, et al., Synthesis, in vitro and in vivo biological evaluation of substituted 3-(5-Imidazo[2,1-b]Thiazolylmethylene)-2-Indolinones as new potent anticancer agents, Eur. J. Med. Chem. 166 (2019) 514–530, https://doi.org/10.1016/j.ejmech.2019.01.049.

[11] A. Andreani, S. Burnelli, M. Granaiola, A. Leoni, A. Locatelli, R. Morigi, M. Rambaldi, L. Varoli, L. Landi, C. Prata, et al., Antitumor activity of bis-indole derivatives, J. Med. Chem. 51 (2008) 4563–4570, https://doi.org/10.1021/jm800194k.
[12] A. Andreani, S. Burnelli, M. Granaiola, A. Leoni, A. Locatelli, R. Morigi, M. Rambaldi, L. Varoli, L. Landi, C. Prata, et al., Antitumor activity and COMPARE analysis of bis-indole derivatives, Bioorg. Med. Chem. 18 (2010) 3004–3011, https://doi.org/10.1016/j.bmc.2010.03.063.
[13] R. Morigi, E. Catanzaro, A. Locatelli, C. Calcabrini, V. Pellicioni, A. Leoni, C. Fimognari, Synthesis and biological evaluation of new bis-indolinone derivatives endowed with cytotoxic activity, Molecules 26 (2021) 6277, https://doi.org/10.3390/molecules26206277.
[14] T. Grunewald, J.A. Ledermann, Targeted therapies for ovarian cancer, Best Pract. Res. Clin. Obstet. Gynaecol. 41 (2017) 139–152, https://doi.org/10.1016/j.bpobgyn.2016.12.001.
[15] J. Bénard, J. Da Silva, M.C. De Blois, P. Boyer, P. Duvillard, E. Chiric, G. Riou, Characterization of a human ovarian adenocarcinoma line, IGROV1, in tissue culture and in nude mice, Cancer Res. 45 (1985) 4970–4979.
[16] C.M. Beaufort, J.C.A. Helmijr, A.M. Piskorz, M. Hoogstraat, K. Ruigrok-Ritstier, N. Besselink, M. Murtaza, W.F.J. van IJcken, A.A.J. Heine, M. Smid, et al., Ovarian cancer cell line panel (OCCP): clinical importance of in vitro morphological subtypes, PLoS One 9 (2014) e103988, https://doi.org/10.1371/journal.pone.0103988.
[17] F.M. Frame, A.R. Noble, P. O'Toole, J. Marrison, T. Godden, A. O'Brien, N. J. Maitland, Assessing the advantages, limitations and potential of human primary prostate epithelial cells as a pre-clinical model for prostate cancer research, Adv. Exp. Med. Biol. 1164 (2019) 109–118, https://doi.org/10.1007/978-3-030-22254-3_9.
[18] M.A. Zaimy, N. Saffarzadeh, A. Mohammadi, H. Pourghadamyari, P. Izadi, A. Sarli, L.K. Moghaddam, S.R. Paschepari, H. Azizi, S. Torkamandi, et al., New methods in the diagnosis of cancer and gene therapy of cancer based on nanoparticles, Cancer Gene Ther. 24 (2017) 233–243, https://doi.org/10.1038/cgt.2017.16.
[19] T. Kouzarides, Chromatin modifications and their function, Cell 128 (2007) 693–705, https://doi.org/10.1016/j.cell.2007.02.005.
[20] Z. Wang, C. Zang, J.A. Rosenfeld, D.E. Schones, A. Barski, S. Cuddapah, K. Cui, T.-Y. Roh, W. Peng, M.Q. Zhang, et al., Combinatorial patterns of histone acetylations and methylations in the human genome, Nat. Genet. 40 (2008) 897–903, https://doi.org/10.1038/ng.154.
[21] C.J. Sherr, D. Beach, G.I. Shapiro, Targeting CDK4 and CDK6: from discovery to therapy, Cancer Discov. 6 (2016) 353–367, https://doi.org/10.1158/2159-8290.CD-15-0894.
[22] G. Tchakarska, B. Sola, The double dealing of cyclin D1, Cell Cycle 19 (2020) 163–178, https://doi.org/10.1080/15384101.2019.1706903.
[23] J.W. Harper, G.R. Adami, N. Wei, K. Keyomarsi, S.J. Elledge, The P21 cdk-interacting protein Cip1 is a potent inhibitor of G1 cyclin-dependent kinases, Cell 75 (1993) 805–816, https://doi.org/10.1016/0092-8674(93)90499-G.
[24] J.S. Desgrosellier, D.A. Cheresh, Integrins in cancer: biological implications and therapeutic opportunities, Nat. Rev. Cancer 10 (2010) 9–22, https://doi.org/10.1038/nrc2748.
[25] M.A. Schwartz, M.H. Ginsberg, Networks and crosstalk: integrin signalling spreads, Nat. Cell Biol. 4 (2002) E65–E68, https://doi.org/10.1038/ncb0402-e65.
[26] C.C. Park, H. Zhang, M. Pallavicini, J.W. Gray, F. Baehner, C.J. Park, M.J. Bissell, B1 integrin inhibitory antibody induces apoptosis of breast cancer cells, inhibits growth, and distinguishes malignant from normal phenotype in three dimensional cultures and *in vivo*, Cancer Res. 66 (2006) 1526–1535, https://doi.org/10.1158/0008-5472.CAN-05-3071.
[27] V. Bhaskar, D. Zhang, M. Fox, P. Seto, M.H. Wong, P.E. Wales, D. Powers, D. T. Chao, R.B. DuBridge, V.A. Ramakrishnan, Function blocking anti-mouse integrin A5β1 antibody inhibits angiogenesis and impedes tumor growth in vivo, J. Transl. Med. 5 (2007) 61, https://doi.org/10.1186/1479-5876-5-61.
[28] V. Bhaskar, M. Fox, D. Breinberg, M.H.-L. Wong, P.E. Wales, S. Rhodes, R. B. DuBridge, V. Volociximab Ramakrishnan, A chimeric integrin Alpha5beta1 antibody, inhibits the growth of VX2 tumors in rabbits, Invest. N. Drugs 26 (2008) 7–12, https://doi.org/10.1007/s10637-007-9078-z.
[29] Z. Li, X. Jiao, C. Wang, L.A. Shirley, H. Elsaleh, O. Dahl, M. Wang, E. Soutoglou, E. S. Knudsen, R.G. Pestell, Alternative cyclin D1 splice forms differentially regulate the DNA damage response, Cancer Res. 70 (2010) 8802–8811, https://doi.org/10.1158/0008-5472.CAN-10-0312.
[30] S. Jirawatnotai, Y. Hu, W. Michowski, J.E. Elias, L. Becks, F. Bienvenu, A. Zagozdzon, T. Goswami, Y.E. Wang, A.B. Clark, et al., A function for cyclin D1 in DNA repair uncovered by protein interactome analyses in human cancers, Nature 474 (2011) 230–234, https://doi.org/10.1038/nature10155.
[31] F. Marampon, G. Gravina, X. Ju, A. Vetuschi, R. Sferra, M.C. Casimiro, S. Pompili, C. Festuccia, A. Colapietro, E. Gaudio, et al., Cyclin D1 silencing suppresses tumorigenicity, impairs DNA double strand break repair and thus radiosensitizes androgen-independent prostate cancer cells to DNA damage, Oncotarget 7 (2016) 5383–5400, https://doi.org/10.18632/oncotarget.6579.
[32] R.D. Clark, J.M. Muchowski, L.E. Fisher, L.A. Flippin, D.B. Repke, M. Souchet, Preparation of indoles and oxindoles from N -(tert -Butoxycarbonyl)-2-Alkylanilines, Synthesis (1991) 871–878, https://doi.org/10.1055/s-1991-26597.
[33] S. Sakai, N. Aimi, A. Kubo, M. Kitagawa, M. Hanasawa, K. Katano, K. Yamaguchi, J. Haginiwa, Structure of gardneramine and 18-demethylgardneramine, Chem. Pharm. Bull. 23 (1975) 2805–2817, https://doi.org/10.1248/cpb.23.2805.
[34] B.V. Silva, N.M. Ribeiro, A.C. Pinto, M.D. Vargas, L.C. Dias, Synthesis of ferrocenyl oxindole compounds with potential anticancer activity, J. Braz. Chem. Soc. 19 (2008) 1244–1247, https://doi.org/10.1590/S0103-50532008000700003.
[35] A. Zakrzewska, E. Kolehmainen, B. Osmialowski, R. Gawinecki, 4-Fluoroanilines: synthesis and decomposition, J. Fluor. Chem. 111 (2001) 1–10, https://doi.org/10.1016/S0022-1139(01)00401-8.
[36] Sampson, P.B.; Liu, Y.; Li, S.-W.; Forrest, B.T.; Pauls, H.W.; Edwards, L.G.; Feher, M.; Patel, N.K.B.; Laufer, R.; Pan, G. Kinase Inhibitors and Method of Treating Cancer with Same 2011. WO2011123946A1.
[37] C. Crestini, R. Saladino, A new efficient and mild synthesis of 2-sxindoles by one-pot wolff-kishner like reduction of isatin derivatives, Synth. Commun. 24 (1994) 2835–2841, https://doi.org/10.1080/00397919408010603.
[38] A. Andreani, M. Granaiola, A. Leoni, A. Locatelli, R. Morigi, M. Rambaldi, V. Garaliene, Synthesis and antitumor activity of 1,5,6-substituted *E* -3-(2-Chloro-3-Indolylmethylene)-1,3-Dihydroindol-2-Ones, J. Med. Chem. 45 (2002) 2666–2669, https://doi.org/10.1021/jm011123c.
[39] R.R. Poondra, N.J. Turner, Microwave-assisted sequential amide bond formation and intramolecular amidation: a rapid entry to functionalized oxindoles, Org. Lett. 7 (2005) 863–866, https://doi.org/10.1021/ol0473804.
[40] L.K. Mehta, J. Parrick, F. Payne, Preparation of 3-ethyloxindole-4,7-quinone, J. Chem. Res. (1998) 190–191, https://doi.org/10.1039/A707530H.
[41] R. Huisgen, H. König, A.R. Lepley, X.V.I.I.I. Nucleophile Aromatische Substitutionen, Neue ringschlüsse über arine, Chem. Ber. 93 (1960) 1496–1506, https://doi.org/10.1002/cber.19600930708.
[42] A. Andreani, M. Rambaldi, D. Bonazzi, L. Greci, F. Andreani, Study on compounds with potential antitumor activity. III. Hydrazone derivatives of 5-substituted 2-chloro-3-formyl-6-methylindole, Farmaco Sci 34 (1979) 132–138, https://doi.org/10.1002/chin.197924211.
[43] J. Amato, R. Morigi, B. Pagano, A. Pagano, S. Ohnmacht, A. De Magis, Y.-P. Tiang, G. Capranico, A. Locatelli, A. Graziadio, et al., Toward the development of specific G-quadruplex binders: synthesis, biophysical, and biological studies of new hydrazone derivatives, J. Med. Chem. 59 (2016) 5706–5720, https://doi.org/10.1021/acs.jmedchem.6b00129.
[44] A. Monks, D. Scudiero, P. Skehan, R. Shoemaker, K. Paull, D. Vistica, C. Hose, J. Langley, P. Cronise, A. Vaigro-Wolff, et al., Feasibility of a high-flux anticancer drug screen using a diverse panel of cultured human tumor cell lines, JNCI Journal of the National Cancer Institute 83 (1991) 757–766, https://doi.org/10.1093/jnci/83.11.757.
[45] G. Micheletti, N. Calonghi, G. Farruggia, E. Strocchi, V. Palmacci, D. Telese, S. Bordoni, G. Frisco, C. Boga, Synthesis of novel structural hybrids between aza-heterocycles and azelaic acid moiety with a specific activity on osteosarcoma cells, Molecules 25 (2020) 404, https://doi.org/10.3390/molecules25020404.
[46] R. Agami, R. Bernards, Distinct initiation and maintenance mechanisms cooperate to induce G1 cell cycle arrest in response to DNA damage, Cell 102 (2000) 55–66, https://doi.org/10.1016/S0092-8674(00)00010-6.
[47] L.L. Pontano, P. Aggarwal, O. Barbash, E.J. Brown, C.H. Bassing, J.A. Diehl, Genotoxic stress-induced cyclin D1 phosphorylation and proteolysis are required for genomic stability, Mol. Cell Biol. 28 (2008) 7245–7258, https://doi.org/10.1128/MCB.01085-08.